PDPO: Parametric Density Path Optimization

Sebastian Gutierrez Hernandez[1] **Peng Chen**[2] **Haomin Zhou**[1]

[1]School of Mathematics, Georgia Institute of Technology
[2]School of Computational Science and Engineering, Georgia Institute of Technology
{shern3, pchen402 ,hmzhou}@gatech.edu

Abstract

We introduce Parametric Density Path Optimization (PDPO), a novel method for computing action-minimizing paths between probability densities. The core idea is to represent the target probability path as the pushforward of a reference density through a parametric map, transforming the original infinite-dimensional optimization over densities to a finite-dimensional one over the parameters of the map. We derive a static formulation of the dynamic problem of action minimization and propose cubic spline interpolation of the path in parameter space to solve the static problem. Theoretically, we establish an error bound of the action under proper assumptions on the regularity of the parameter path. Empirically, we find that using 3–5 control points of the spline interpolation suffices to accurately resolve both multimodal and high-dimensional problems. We demonstrate that PDPO can flexibly accommodate a wide range of potential terms, including those modeling obstacles, mean-field interactions, stochastic control, and higher-order dynamics. Our method outperforms existing state-of-the-art approaches in benchmark tasks, demonstrating superior computational efficiency and solution quality. Source code `https://github.com/SebasGutHdz/PDPO/tree/main` .

1 Introduction

Optimal transport (OT) theory has become a powerful and widely used framework for quantifying discrepancies and constructing interpolations between probability distributions, with rapidly expanding applications in machine learning, statistics, and computational science [27]. It offers a principled way to compare distributions by computing the minimal cost required to transform one distribution into another.

While the computation of optimal transport (OT) plans and geodesics between probability distributions is now relatively well understood [31, 22, 3, 34, 25, 13], many real-world applications require solving more complex, constrained transport problems—specifically, identifying optimal paths between distributions subject to additional requirements. For instance, one may need to guide a swarm of robots from one configuration to another while avoiding obstacles, or interpolate between data distributions in a way that preserves semantic structure [20, 29, 17].

These tasks can be formulated as action-minimizing problems governed by the "principle of least action": Given initial and terminal densities $\rho_0, \rho_1 \in \mathcal{P}(\mathbb{R}^d)$, where $\mathcal{P}(\mathbb{R}^d)$ denotes the space of probability densities over $\mathbb{R}^d$, the objective is to find a time-dependent density path $\rho(t,\cdot) \in \mathcal{P}(\mathbb{R}^d)$ and a continuous velocity field $v : [0,1] \times \mathbb{R}^d \to \mathbb{R}^d$ that minimize the action functional:

$$\inf_{\rho, v} \int_0^1 \int_{\mathbb{R}^d} K(\rho, v)\, dx + F(\rho(t))\, dt \tag{1}$$

$$\text{subject to} \quad \partial_t \rho + \nabla \cdot (\rho v) = 0, \quad \rho(0,\cdot) = \rho_0, \quad \rho(1,\cdot) = \rho_1. \tag{2}$$

39th Conference on Neural Information Processing Systems (NeurIPS 2025).

Here, $K(\rho, v)$ denotes the transportation energy, and $F(\rho)$ represents a potential term that captures interactions among particles or with the environment. When $K(\rho, v) = \frac{1}{2}|v|^2\rho$ and $F(\rho) = 0$, this reduces to the classical Wasserstein geodesic problem. Directly solving such action-minimizing problems poses substantial mathematical and computational challenges. In low dimensions (e.g., 2 or 3), the associated PDE system—derived from the first-order optimality conditions—can be tackled using classical numerical methods [1, 5, 6, 14]. However, these approaches do not scale well with dimension and become computationally infeasible in high-dimensional settings.

Recent advances in machine learning have greatly expanded the range of high-dimensional problems that can be tackled effectively. A leading example is the Generalized Schrödinger Bridge Method (GSBM) [20], originally developed for stochastic optimal control (SOC) problems [24]. GSBM learns forward and backward vector fields by modeling conditional densities and velocities, drawing inspiration from stochastic interpolants [2], and approximates Gaussian path statistics via spline-based optimization. In parallel, [29] introduced an algorithm for problems with linear energy potentials, leveraging Kantorovich duality and amortized inference to efficiently compute c-transforms and transportation costs. For Mean-Field Games, APAC-Net [17] casts the primal-dual formulation as a convex-concave saddle point problem, trained using a GAN-style adversarial framework.

Our method builds upon prior work on parametric probability distributions [21, 33, 15], extending these ideas to address boundary-valued action-minimizing density problems. Our formulation is an extension of the *static OT* formulation to the parameter space, whereas in [16], they extend the *dynamic formulation*. In the remainder of this section, we outline our methodology, with full technical details deferred to Section 3.

Figure 1a offers an overview of our approach: curves in parameter space $\theta(t) \in \Theta$ (left) induce density paths $\rho_t \in \mathcal{P}(\mathbb{R}^d)$ via pushforward maps $\rho_t = (T_{\theta(t)})_{\#}\,\lambda$ from a fixed reference density λ (top), while samples of these densities are obtained via direct evaluation $T_{\theta(t)}(z)$ with $z \sim \lambda$ (right).

While spline-based methods have previously been applied to particle-level density transport [29] and Gaussian settings [20], a key innovation of our work is the use of cubic Hermite splines in the parameter space of a neural network. We fix a set of control points $\{\theta_{t_i}\}_{i=0}^{K+1}$ with $t_i = i/(K+1)$ and optimize over them to discover action-minimizing density paths, which presents the first spline-based parametric approach in a learned map setting. Figures 1b and 1c illustrate our method on an obstacle avoidance task, showing the pushforward of λ at the optimized control points and the resulting continuous path of probability densities.

The optimization of the $K + 2$ control points proceeds in the following steps: **Step 1:** Initialize a pair of boundary parameters, θ_0 and θ_1, that accurately approximate the target boundary densities

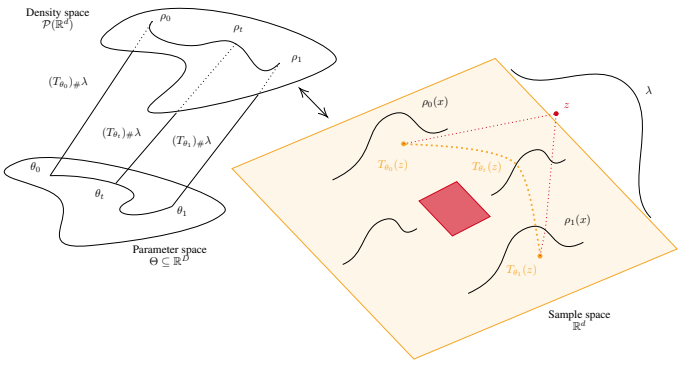

(a) The space of probability densities $\mathcal{P}(\mathbb{R}^d)$ (top), the admissible parameter set $\Theta \subseteq \mathbb{R}^d$ (left), and the sampling space $\mathbb{R}^d$ with an obstacle (right)

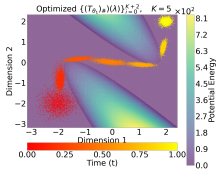

(b) Control points

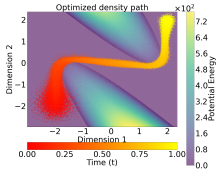

(c) Density path

Figure 1: Visualization of our framework. (a) Illustrates the three main components: the space of probability densities $\mathcal{P}(\mathbb{R}^d)$ (top), the admissible parameter space $\Theta \subseteq \mathbb{R}^d$ (left), and the sampling space $\mathbb{R}^d$ containing an obstacle (right). (b) and (c) depict the pushforwards of the optimized control points $(T_{\theta_i})_{\#}\,\lambda$ for $i = 0, \ldots, K$ and the continuous spline trajectory $(T_{\theta(t)})_{\#}\,\lambda$, respectively. Time is color-coded, with red indicating $t = 0$ and yellow indicating $t = 1$.

ρ_0 and ρ_1. **Step 2:** With the boundary parameters (θ_0, θ_1) fixed, optimize the interior control points $\{\theta_{t_i}\}_{i=1}^{K+1}$ to minimize the action associated with the coupling $(T_{\theta_0}, T_{\theta_1})_{\#}\lambda$. **Step 3:** Optimize the boundary parameters (θ_0, θ_1) in order to improve the quality of the coupling while keeping the interior control points fixed. Repeat steps 2 and 3 iteratively until convergence.

Contributions. Our main contributions are: (1) We introduce Parametric Density Path Optimization (PDPO), a novel framework that transforms infinite-dimensional density path optimization into a finite-dimensional problem by parameterizing pushforward maps with cubic Hermite splines. Our approach achieves accurate density paths with as few as 3–5 control points. (2) We generalize the parametric framework to support a wide class of action-minimizing problems, including stochastic optimal control (via Fisher information), acceleration-regularized dynamics, and mean-field interactions, within a unified optimization scheme based on learned transport maps. (3) We empirically validate PDPO across several challenging benchmarks—including obstacle avoidance, entropy-constrained transport, and high-dimensional opinion dynamics—achieving up to 7% lower action, up to $10\times$ improved boundary accuracy, and 40–80% faster runtimes compared to state-of-the-art baselines.

2 Background

This section presents the mathematical foundations of optimal transport, its dynamic formulation, and parametric methods that enable scalable and efficient application in machine learning contexts.

2.1 Optimal transport and Wasserstein distances

In what follows, we only consider distributions μ that are Lebesgue dominated, thus there is a function $\rho : \mathbb{R}^d \to \mathbb{R}_{\geq 0}$ such that for any measurable set A, $\mu(A) = \int_A \rho(x)dx$. Since we are restricting ourselves to this case, we use the terms distribution and density interchangeably for convenience.

The Wasserstein-2 distance between two probability distributions $\rho_0, \rho_1 \in \mathcal{P}(\mathbb{R}^d)$ is defined as:

$$W_2^2(\rho_0, \rho_1) = \inf_{\pi \in \Pi(\rho_0, \rho_1)} \int_{\mathbb{R}^d \times \mathbb{R}^d} \|x - y\|^2 d\pi(x, y), \tag{3}$$

where $\Pi(\rho_0, \rho_1)$ denotes the set of all joint distributions with marginals ρ_0 and ρ_1 [32].

When ρ_0 is absolutely continuous with respect to the Lebesgue measure, the Benamou–Brenier formulation [4] provides a dynamic reinterpretation of this distance:

$$W_2^2(\rho_0, \rho_1) = \inf_{\rho, v} \int_0^1 \int_{\mathbb{R}^d} \frac{1}{2} \|v(t, x)\|^2 \rho(t, x) dx dt \tag{4}$$

$$\text{subject to} \quad \partial_t \rho + \nabla \cdot (\rho v) = 0, \quad \rho(0, \cdot) = \rho_0, \quad \rho(1, \cdot) = \rho_1. \tag{5}$$

This dynamical formulation interprets the Wasserstein distance as the minimum kinetic energy required to continuously transport the mass of ρ_0 into ρ_1 over the time interval $[0, 1]$.

2.2 Generalized action-minimizing problems in Wasserstein space

We consider the following generalized action-minimizing problem:

$$\inf_{\rho, v} \int_0^1 \int_{\mathbb{R}^d} \frac{1}{2} \|v(t, x)\|^2 \rho(t, x) dx + F(\rho(t))\, dt \tag{6}$$

$$\text{subject to} \quad \partial_t \rho + \nabla \cdot (\rho v) = 0, \quad \rho(0, \cdot) = \rho_0, \quad \rho(1, \cdot) = \rho_1,$$

where the functional $F(\rho)$ incorporates additional constraints or potentials, defined as:

$$F(\rho) = \kappa_0 \int_{\mathbb{R}^d} V(x)\rho(x)dx + \kappa_1 \int_{\mathbb{R}^d} U(\rho(x))dx + \kappa_2 \int_{\mathbb{R}^d \times \mathbb{R}^d} W(x - y)\rho(x)\rho(y)dxdy. \tag{7}$$

Here, the three terms correspond respectively to: external potentials (e.g., obstacles or environmental forces), internal energy (e.g., entropy or Fisher information), and interaction energy (e.g., repulsion or attraction between mass elements). The constants $\kappa_0, \kappa_1, \kappa_2 \in \mathbb{R}_+$ model the strength of each term.

In our setup, the Fisher Information potential, given by

$$\mathcal{FI}(\rho) = \frac{\sigma^4}{8} \int \|\nabla \log \rho\|^2 \rho(x) dx, \tag{8}$$

plays a crucial role. As shown in prior work [11, 23] and detailed in Appendix A, it is well established that the following deterministic control problem:

$$\begin{aligned} &\inf_{\rho, v} \int_0^1 \int_{\mathbb{R}^d} \frac{1}{2} \|v(t,x)\|^2 \rho(t,x) dx + F(\rho(t)) + \mathcal{FI}(\rho(t))\, dt \\ &\quad \text{subject to} \quad \partial_t \rho + \nabla \cdot (\rho v) = 0, \quad \rho(0,\cdot) = \rho_0, \quad \rho(1,\cdot) = \rho_1, \end{aligned}$$

is equivalent to the stochastic optimal control (SOC) problem:

$$\begin{aligned} &\inf_{\rho, v} \int_0^1 \int_{\mathbb{R}^d} \frac{1}{2} \|v(t,x)\|^2 \rho(t,x) dx + F(\rho(t))\, dt \\ &\quad \text{subject to} \quad \partial_t \rho + \nabla \cdot (\rho v) = \frac{\sigma^2}{2} \Delta \rho, \quad \rho(0,\cdot) = \rho_0, \quad \rho(1,\cdot) = \rho_1. \end{aligned}$$

This equivalence allows us to recast SOC problems as deterministic action-minimization tasks augmented with a Fisher Information regularization term. While the deterministic action-minimization formulation offers a principled framework for modeling action-minimizing dynamics, directly solving the resulting infinite-dimensional optimization problem over probability densities is computationally prohibitive in high dimensions. To address this, we next introduce parametric representations that reduce the problem to a finite-dimensional setting, enabling tractable and scalable computation.

2.3 Parametric pushforward representations of probability densities

To render action-minimizing problems computationally tractable, we focus on parameterized families of probability distributions, thereby reducing the original infinite-dimensional optimization problem to a finite-dimensional one over the parameter space. This strategy builds on recent developments in parameterized Wasserstein dynamics for solving initial-value Hamiltonian systems and gradient flows [33, 15].

The work most closely related to our approach is that of [8], which formulates the Schrödinger Bridge (SB) problem between Gaussian distributions as an action-minimization task. Leveraging the fact that the SB solution between Gaussians remains Gaussian, they parameterize the evolving density by its mean and covariance, and derive Euler–Lagrange equations for these parameters by projecting the density-level optimality conditions onto the parametric space.

We now introduce the core elements of our parametric pushforward formulation, starting with the definition of some key concepts. For further background, we refer the reader to [33, 16].

Definition 1. *We consider a **parameter space** $\Theta \subseteq \mathbb{R}^D$ of dimension D. We call $T : \mathbb{R}^d \times \Theta \to \mathbb{R}^d$ a **parametric mapping**, if for every $\theta \in \Theta$, the function $T(\cdot, \theta)$, or $T_\theta(\cdot)$ used interchangeably, is Lebesgue measurable. The corresponding **parametric density space** is defined as*

$$P_\Theta := \{\rho_\theta = (T_\theta)_\# \lambda : \theta \in \Theta\} \subseteq \mathcal{P}(\mathbb{R}^d),$$

*where $(T_\theta)_\# \lambda$ denotes the pushforward of a fixed reference density λ under the map T_θ, see Figure 1a(top). Moreover, given a curve in the parameter space $\theta(t) \in \Theta$ indicated by $t \in [0,1]$, the corresponding **pushforward density path** is defined as $\rho_{\theta(t)} := (T_{\theta(t)})_\# \lambda$, see Figure 1a(top), and the **sample trajectories** are given by $x_{\theta(t)}(z) = T_{\theta(t)}(z), z \sim \lambda$, see Figure 1a(right).*

3 Action Minimizing Problems via Parametric Pushforwards

3.1 Projection of the action-minimizing problem to the parametric setting

To motivate our framework, we begin by revisiting an alternative formulation of the classical Wasserstein-2 distance defined in (3). Given $x, y \in \mathbb{R}^d$, define the set of admissible paths $\Gamma(x,y) := \big\{\gamma(t) \in C^1([0,1], \mathbb{R}^d) : \gamma(0) = x, \gamma(1) = y\big\}$. Then the classical formula

$$\|x - y\|^2 = \inf_{\gamma(t) \in \Gamma(x,y)} \int_0^1 \|\gamma'(t)\|^2 dt,$$

allows us to write the Wasserstein-2 distance as

$$W_2^2(\rho_0, \rho_1) = \inf_{\pi \in \Pi(\rho_0, \rho_1)} \int_{\mathbb{R}^d \times \mathbb{R}^d} \inf_{\gamma(t) \in \Gamma(x,y)} \int_0^1 \|\gamma'(t)\|^2 \, dt \, d\pi(x, y). \tag{9}$$

In other words, one first chooses a coupling π between the endpoints and then pays, for each pair (x, y), the minimal kinetic energy needed to drive a particle from x to y. Our framework adopts exactly this viewpoint: we cast the dynamic optimization in (6) as a static coupling problem whose cost is still evaluated via a dynamic (least-action) criterion.

For generalized action-minimizing problems, the action of a path is

$$\mathcal{A}(\gamma) = \mathbb{E}_{x \sim \rho_0} \left[\int_0^1 \left\| \frac{d}{dt} \gamma_t(x) \right\|^2 dt \right] + \int_0^1 F(\rho_{\gamma_t}) dt. \tag{10}$$

We make the following restrictions to guarantee the existence of the density in all the trajectories of a coupling. Define the set

$$\mathcal{T}_{\rho_0, \rho_1} = \{T : \mathbb{R}^d \to \mathbb{R}^d : T \text{ diffeomorphic}, T_\#(\rho_0) = \rho_1, \det(DT) > 0\}.$$

Since the ρ_0 and ρ_1 have densities, the Monge map T^* is a diffeomorphism that satisfies $\det(DT) > 0$ [4] and the set $\mathcal{T}_{\rho_0, \rho_1} \neq \emptyset$. If $T \in \mathcal{T}_{\rho_0, \rho_1}$ then it is smoothly isotopic to the identity id, see Lemma 2, Chapter 6 [7]. By the definition of diffeomorphism being smoothly isotopic, for maps $T \in \mathcal{T}_{\rho_0, \rho_1}$, the set $\Gamma(\pi)$ consisting of the flow maps $\gamma \in C^1([0, 1] \times \mathbb{R}^d, \mathbb{R}^d)$, such that $\gamma_t(x) := \gamma(t, x)$ describes the position at time t of a particle starting at x, i.e., $\gamma_0(x) = x$, $\gamma_t(\cdot)$ is diffeomorphic for each $t \in [0, 1]$, and $(\gamma_0, \gamma_1)_\# \, \rho_0 = \pi$ is non-empty. We also define the set of couplings

$$\tilde{\Pi} = \{\pi \in \Pi(\rho_0, \rho_1) : \pi = (id, T_\pi)_\#(\rho_0) \text{ for some map } T_\pi \in \mathcal{T}_{\rho_0, \rho_1}\}.$$

accumulated potential over the evolving density path. The cost associated with a coupling $\pi \in \tilde{\Pi}$ is then defined as

$$c(\pi) = \inf_{\gamma \in \Gamma(\pi)} \mathcal{A}(\gamma).$$

Our primary objective is the following action-minimizing problem:

$$\inf_{\pi \in \tilde{\Pi}(\rho_0, \rho_1)} c(\pi) = \inf_{\pi \in \tilde{\Pi}(\rho_0, \rho_1)} \inf_{\gamma \in \Gamma(\pi)} \mathcal{A}(\gamma). \tag{11}$$

To the best of our knowledge, this formulation is novel. While related ideas appear in [29] and [32], those works are limited to linear potentials or "lifted" Lagrangians. In contrast, our formulation includes internal and interaction energy terms, which significantly alter the structure of the problem. In particular, the cost of each particle trajectory depends not only on its velocity and position, but also on the global density path ρ_t.

The following theorem, whose proof can be found in Appendix B, establishes the equivalence between the dynamic and static formulations given in Equations (6) and (11), respectively.

Theorem 1. *The dynamic formulation in Equation* (6) *is equivalent to the static formulation in Equation* (11)*.*

With these definitions in place, we now formulate the action-minimizing problem from a parametric perspective. Let the parameter space Θ, the parametric map T, and the reference density λ be fixed. Define the set of admissible boundary parameters as

$$\Theta_0^1 = \left\{(\theta_0, \theta_1) \in \mathbb{R}^D \times \mathbb{R}^D : (T_{\theta_i})_\# \, \lambda = \rho_i, i = 0, 1\right\}.$$

Given a parameter curve with boundary condition $\theta_{0 \to 1} \in \Theta_{0 \to 1} := \{\theta_{0 \to 1} \in C^1([0, 1], \Theta) : \theta(0) = \theta_0, \theta(1) = \theta_1\}$, we define its action (by slight abuse of notation) as

$$\mathcal{A}(\theta_{0 \to 1}) := \mathbb{E}_{z \sim \lambda} \left[\int_0^1 \left\| \frac{d}{dt} T_{\theta(t)}(z) \right\|^2 dt \right] + \int_0^1 F((T_{\theta(t)})_\# \, \lambda) dt, \tag{12}$$

where $T_{\theta(t)}(z)$ denotes the transported trajectory at t of a particle z drawn from the reference distribution with density λ. The corresponding parametric action-minimization problem is given by:

$$\inf_{(\theta_0,\theta_1)\in\Theta_0^1} \inf_{\theta_{0\to1}\in\Theta_{0\to1}} \mathcal{A}(\theta_{0\to1}). \tag{13}$$

This formulation parallels the coupling-based problem in Equation (11) but operates directly in the parameter space of the transport maps.

While [16] explored the Lagrangian formulation of Equation (6) in parameter space from a theoretical perspective, our approach in Equation (13) introduces an alternative formulation based on coupling costs. This perspective not only offers conceptual clarity but also lends itself naturally to numerical implementation.

Motivated by [20], we employ cubic Hermite spline approximation of the parameter curve $\theta_{0\to1}$ in solving the optimization problem (13). The following theorem provides an estimate for the error introduced in the objective action. The full set of assumptions and proof are provided in Appendix C.

Theorem 2. *Let $\theta_{0\to1}$ be a parameter curve with $l \geq 1$ continuous derivatives, and let $\tilde{\theta}_{0\to1}$ be its cubic Hermite spline approximation using K uniformly spaced control (collocation) points. Then the error in the action satisfies $|\mathcal{A}[\theta_{0\to1}] - \mathcal{A}[\tilde{\theta}_{0\to1}]| = O(h^{\kappa-1})$, where $\kappa := \min(l, 4)$.*

While action-minimizing curves can be computed analytically or via numerical integration for simple parametric families (e.g., affine maps) and linear potentials (see [33]), such formulations are inherently limited in expressivity. To overcome this, we adopt Neural ODEs [9] as flexible and expressive parametric maps for modeling complex density dynamics.

3.2 Pushforward map via Neural ODE

Neural Ordinary Differential Equations (Neural ODEs) [9] define continuous-time transformations via parameterized differential equations:

$$\frac{d\psi(\tau, z)}{d\tau} = v_\theta(\tau, \psi(\tau, z)), \quad \psi(0, z) = z \sim \lambda, \tag{14}$$

where $v_\theta : [0, 1] \times \mathbb{R}^d \to \mathbb{R}^d$ is a neural network parameterized by θ, λ is typically a standard normal distribution, and τ denotes the ODE time variable. The resulting transport map is defined as:

$$T_\theta(z) = z + \int_0^1 v_\theta(\tau, \psi(\tau, z))\, d\tau. \tag{15}$$

We adopt Neural ODEs as parametric maps due to their ability to support efficient computation of both the entropy $\log(\rho)$ and the score $\nabla_x \log(\rho)$ through auxiliary ODE systems [35]. Details of these complementary entropy and score equations are provided in Appendix D.

3.3 Optimization framework

The static formulation (13) defines a bilevel optimization problem: the boundary conditions ensure feasibility by satisfying $(T_{\theta_i})_\# \lambda = \rho_i, i = 0, 1$. The curve $\theta_{0\to1}$ minimizes the action and determines the coupling cost. From the perspective of the spline control points $\{\theta_{t_i}\}_{i=0}^{K+1}$, the boundary parameters are θ_0, θ_1, while the interior path is defined by $\{\theta_{t_i}\}_{i=1}^{K}$. This motivates our optimization strategy:

Step 1: Initialization. First, initialize the boundary parameters θ_0 and θ_1 such that $(T_{\theta_i})_\# \lambda$ are good approximations of ρ_i for $i = 0, 1$. We employ Flow Matching (FM) for its efficiency. We in general consider this step outside of the main algorithm. In Table 1 we include in the last column the FM training times. A parameter can be used for any functional, so once a boundary parameter has been obtained, it can be reused across multiple problems, see Appendix F.1.2. Second, initialize the control points $\{\theta_{t_i}\}_{i=1}^{K}$ as the linear interpolation of θ_0 and θ_1. Then run a few iterations of path optimization with $F(\rho) = 0$. In Appendix F.1.1 and Appendix F.2, we show the computational advantages of each part of the initialization step.

Step 2: Path optimization. Perform a gradient-based path optimization to update the interior control points $\{\theta_{t_i}\}_{i=1}^{K}$ to minimize the action (12), while keeping the boundary parameters fixed, see details

in Algorithm 1. The action functional (12) is evaluated using the trapezoidal rule with N time steps and M Monte Carlo samples. The gradient is computed using automatic differentiation. See Algorithm 1

Step 3: Boundary/coupling optimization. Optimize the boundary parameters (θ_0, θ_1) while keeping the interior spline control points $\{\theta_{t_i}\}_{i=1}^{K}$ fixed, see details in Algorithm 2. Specifically, we formulate this as a penalized optimization problem:

$$\min_{\theta_0,\theta_1\in\Theta} \mathbb{E}_{z\sim\lambda}\left[\sum_{i=0}^{1}\alpha_i L((T_{\theta_i})_{\#}\,\lambda,\rho_i)\right] + \mathcal{A}[\theta_{0\to 1}]. \tag{16}$$

Here L is a dissimilarity metric between distributions, for which we use the FM loss function. The weights α_i, $i = 0, 1$, balance boundary accuracy and coupling optimality. The action $\mathcal{A}[\theta_{0\to 1}]$ (12) is added as a penalty term, which is estimated at the current control points, see Algorithm 2

We repeat the optimizations of step 2 and step 3 alternatively until convergence, producing both an optimal coupling and a minimal-action path between ρ_0 and ρ_1, see Algorithm 3. Observe as long as the action is lower bounded, step 2 will converge to a local minimum. The dissimilarity is assumed to be nonnegative, thus step 3 also converges to a local minimum.

4 Experiments

We conduct a comprehensive evaluation of our method across a variety of benchmark scenarios to demonstrate its accuracy, efficiency, flexibility, and scalability. In all experiments, we compare against GSBM [20], the current state-of-the-art, which has been shown to outperform earlier approaches. Where appropriate, we also include comparisons with Neural Lagrangian Optimal Transport (NLOT) [29] and APAC-Net [17]. It is important to note that NLOT is limited to linear potentials, while APAC-Net is specifically designed for mean-field games (MFG) and employs soft terminal costs instead of enforcing hard distributional constraints.

In F.3 we include an ablation study on the number of control points.

4.1 Implementation details

We implement our method in PyTorch [28], and run all experiments on an AMD 7543 CPU + NVIDIA RTX A6000 GPU. The Wasserstein-2 distance is approximated using the POT library [12] with 3,000 samples. For estimating the action, we use Monte Carlo integration with 3,000 samples and compute the time integral using the trapezoidal rule with a step size of $\Delta t = 1/50$. Each experiment is repeated across three random trials with different seeds. Additional implementation and experimental details are provided in Appendix F. In Table 4 see the boundary conditions ρ_0 and ρ_1, and Table 4 the hyper-parameters for the PDPO algorithm.

4.2 Obstacle avoidance with mean-field interactions

We demonstrate the effectiveness of our method through three challenging obstacle avoidance scenarios involving mean-field interactions. See Appendix F.4 for their mathematical definitions.

S-Curve with Congestion (SCC) from [17]: Particles navigate around two obstacles arranged in an "S"-shaped configuration while interacting with one another. PDPO achieves superior performance compared to existing methods (GSBM and APAC-Net), yielding lower action values, more accurate boundary approximation, and faster runtimes (see Table 1).

Notably, the interpolated density path generated by PDPO (Figure 2b) exhibits clear nonlinearity between control points. As shown in Figure 2a, a linear interpolation of the density between control points θ_{t_1} (red) and θ_{t_2} (orange) would intersect the obstacles. This highlights how PDPO's spline-based parameterization effectively exploits the geometry of the parameter space to avoid infeasible paths. Note that both GSBM and APAC-Net violate the obstacle avoidance constraint in this scenario.

V-Neck with Entropy and Fisher Information (VNEFI) from [20]: This stochastic optimal control (SOC) problem involves particles navigating a narrow channel while minimizing entropy, see Figure 11b. PDPO outperforms GSBM by achieving lower action values, comparable boundary accuracy, and significantly faster runtime (see Table 1). When GSBM is restricted to the same runtime as

Table 1: Comparison for obstacle avoidance with mean-field interactions. The quantities $W_2(\rho_i)$ $i = 0, 1$ denote the empirical are the Wasserstein-2 distances at times computed using the POT library [12]. The FM time is the sum of the FM training times for both boundaries.

Problem (method)	$\mathcal{A}[\rho_t]$	$\int_0^1 \mathbb{E}_{\rho_t} V(X)dt$	$(W_2(\rho_0), W_2(\rho_1))$	Time	FM Time
SCC (PDPO)	$\mathbf{39.90 \pm 0.16}$	1.12 ± 0.02	$(\mathbf{0.028}, \mathbf{0.014})$	**11m**	134s
SCC (GSBM)	$40.02 \pm .75$	4.05 ± 1.48	$(0.21, 0.25)$	21m	-
SCC (Apac-net)	39.95 ± 0.25	1.31 ± 0.16	$(0, 0.093)$	12m	-
VNEFI (PDPO)	$\mathbf{148.91 \pm 0.72}$	38.290 ± 0.43	$(\mathbf{0.082}, 0.078)$	**70m**	77s
VNEFI (GSBM)	156.80 ± 4.31	74.28 ± 1.23	$(0.086, \mathbf{0.062})$	115m	-
GMM (PDPO)	$\mathbf{79.46 \pm 0.62}$	0.41 ± 0.35	$(0, 0.359)$	**8m**	3m10s
GMM (GSBM)	88.77 ± 3.31	14.59 ± 3.26	$(0.806, \mathbf{0.258})$	123m	-
GMM (NLOT)	82.06 ± 2.80	0.006 ± 0.006	$(0, 0.629)$	117m	-

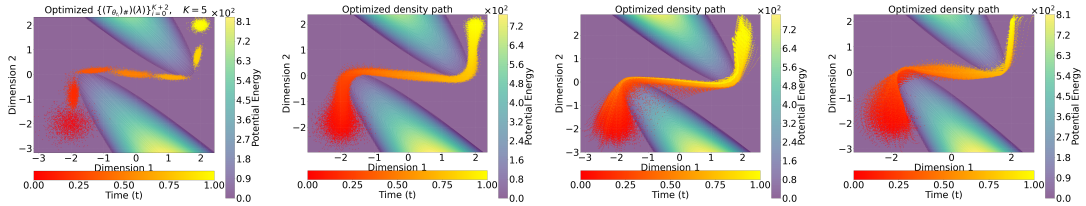

(a) $(T_{\theta_{t_i}})_{\#}\,\lambda$ (b) PDPO $(T_{\theta_t})_{\#}\,\lambda$ (c) GSBM (d) APAC-Net

Figure 2: S-curve-C: (a) Pushforward densities at control points, (b) Pushforward densities along the interpolated trajectory, (c) Density path produced by GSBM, (d) Density path produced by APAC-Net

PDPO (details in Appendix F.4), its action value remains similar, but its boundary approximation deteriorates by an order of magnitude.

Gaussian Mixture obstacle (GMM) from [20]: In this benchmark, particles must move between multimodal source and target distributions while avoiding a Gaussian mixture-shaped obstacle, see Figure 13 for the density path in the appendix. This example demonstrates PDPO's flexibility in selecting different reference distributions. By setting the reference distribution $\lambda = \rho_0$, there is no approximation error at time $t = 0$. In Table 1 we compare against GSBM and NLOT. Our approach achieves a slight improvement of 0.04% in the action, but the computational time was reduced by approximately 85% from nearly 2 hours to less than 10 minutes. While GSBM achieves a marginally better boundary representation for ρ_1, our method offers comparable optimization quality with substantially faster computation.

Note that for GSBM, the reported $W_2(\rho_0)$ values are computed by evolving samples drawn from ρ_1 via the backward SDE to obtain the empirical approximation of ρ_0

4.3 Generalized momentum minimization

Building on the momentum Schrödinger Bridge (SB) framework by [10], we extend action-minimizing problems to incorporate acceleration alongside additional potential terms. This leads to a novel formulation that minimizes the following objective:

$$\mathcal{A}(\gamma) = \mathbb{E}_{x\sim\rho_0}\left[\int_0^1 \left\|\frac{d^2}{dt^2}\gamma_t(x)\right\|^2 dt\right] + \int_0^1 F(\rho_{\gamma_t})dt.$$

Figure 3 illustrates PDPO solutions for the obstacle avoidance with mean-field interaction class of problems. The resulting paths are noticeably smoother, compare the top and bottom rows of Figure 3

To our knowledge, no prior method has addressed these generalized settings within a unified momentum formulation, underscoring PDPO's flexibility beyond classical Wasserstein geodesics.

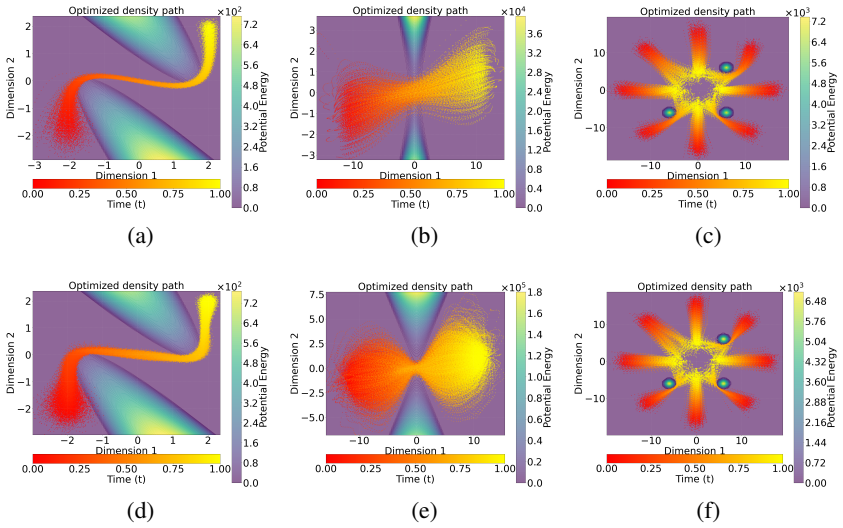

Figure 3: Solutions for generalized momentum-minimizing problems (a-c). Solutions for kinetic energy minimizing problems (d-f).

4.4 High-dimensional opinion depolarization

We examine the opinion depolarization problem following [30] and [19]. Here, $\rho(t,\cdot) : \mathbb{R}^d \to \mathbb{R}_{\geq 0}$ models the opinion density of a population, where each coordinate represents an agent's opinion on a topic. The particle-level opinion dynamics evolve as

$$\frac{dx(t)}{dt} = \frac{f_{\text{polarize}}(x(t); \rho(t,\cdot))}{\|f_{\text{polarize}}(x(t); \rho(t,\cdot))\|},$$

with

$$f_{\text{polarize}}(x; \rho(t,\cdot), \xi_t) := \mathbb{E}_{y\sim p_t}[a(x,y,\xi_t)\vec{y}], \quad a(x,y,\xi_t) := \begin{cases} 1 & \text{if } \text{sign}(\langle x, \xi_t\rangle) = \text{sign}(\langle y, \xi_t\rangle) \\ -1 & \text{otherwise} \end{cases}.$$

The function $a(x, y; \xi)$ evaluates opinion alignment at random information ξ sampled independently of $\rho(t,\cdot)$. These dynamics cause an unpolarized initial condition $\rho(0,\cdot)$ (e.g., Gaussian) to polarize into opinion clusters. We seek a velocity $v(t,x)$ preventing polarization by enforcing an unpolarized terminal condition $\rho(1,\cdot)$ (see Appendix F.5).

The action is

$$\mathcal{A}_{\text{polarize}}(\theta_{0\to 1}) := \mathbb{E}_{z\sim\lambda}\left[\frac{1}{2}\|f_{\text{polarize}}(T_{\theta(t)}(z); (T_{\theta(t)})_{\#}(\lambda)) - \frac{d}{dt}T_{\theta(t)}(z)\|^2\right] + \int_0^1 F((T_{\theta(t)})_{\#}(\lambda))dt.$$

Figure 4 shows PDPO achieves quality comparable to [20], as evidenced by 2D PCA projections and directional similarity histograms at terminal time. These histograms show cosine similarity distributions between opinion vector pairs, measuring alignment independent of magnitude. PDPO's key advantage is computational efficiency: completing in 23 minutes versus over 5 hours for GSBM. We attribute this success to: (1) the spline path $\theta_{0\to 1}$ readily reaches the non-polarized target at $t = 1$ from initialization, and (2) it connects boundary conditions independently of f_{polarize}. Note that training boundary conditions θ_0 and θ_1 required 29m35s and 31m12s, respectively.

5 Computational complexity and limitations

The primary computational cost in our algorithm arises from pushforward evaluations. When the action integral is approximated using N time points, our method requires evaluating N Neural ODEs (NODEs). Each NODE involves integrating a velocity field using 10 time steps. For expectation estimates, we use M Monte Carlo samples per NODE.

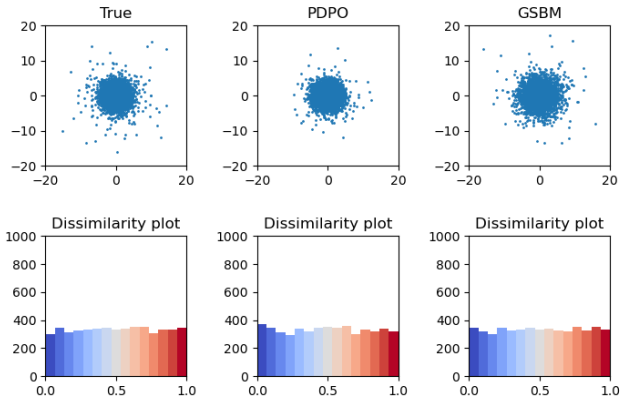

Figure 4: Opinion depolarization in 1000 dimensions. Top: 2D PCA projections of the distributions. Bottom: directional similarity histograms. Left: target unimodal distribution. Middle: PDPO solution. Right: DeepGSB solution.

When the functional F includes entropy and Fisher Information terms, the cost increases substantially. Computing the entropy requires solving an additional 1D ODE, while the Fisher Information involves a separate d-dimensional ODE, where d is the problem dimension. In total, this results in $O(N \times M \times (1+d))$ ODE evaluations for problems involving both terms.

In Appendix F.6 , we showcase the scalability of our method with a 50-dimensional Schrödinger Bridge example, representing the highest-dimensional case with Fisher Information we have successfully computed.

Currently, our implementation is limited to NODEs with MLP architectures, see Appendix F, which limits applications to image-based transport problems, unlike GSBM [20].

6 Conclusions

We introduced Parametric Density Path Optimization (PDPO), a general framework for solving action-minimizing problems over probability densities by leveraging parameterized pushforward maps. This approach transforms the original infinite-dimensional optimization over density paths into a tractable, finite-dimensional problem in parameter space, using cubic splines with a small number of control points.

A central conceptual distinction of PDPO is that its outcome is not a single trained neural network, but a collection of $K+1$ trained models $\{T_{\theta_{t_i}}\}_{i=0}^{K}$ whose parameters lie on a spline-defined trajectory. Together, these models define a continuous transformation in density space through the pushforward of the interpolated parameters. From this perspective, PDPO learns a dynamical path in the parameter space, a time-dependent family of mappings that approximate the evolution of the probability mass.

Experimental results show that PDPO matches or surpasses state-of-the-art methods in accuracy, while requiring substantially less computation time.

7 Broader Impact

The study of action-minimizing problems in density space might have applications in the study of population dynamics.

Acknowledgments and Disclosure of Funding

Chen acknowledges partial support from NSF #2325631, #2245111. This research is partially supported by NSF grant DMS-230746. The authors would also like to acknowledge Benjamin Burns for the helpful discussions and the rendering of Figure 1a and Shu Liu for the helpful discussions.

References

[1] Yves Achdou and Italo Capuzzo-Dolcetta. Mean Field Games: Numerical Methods. *SIAM Journal on Numerical Analysis*, 48(3):1136–1162, January 2010. ISSN 0036-1429, 1095-7170. doi: 10.1137/090758477. URL http://epubs.siam.org/doi/10.1137/090758477.

[2] Michael S. Albergo, Nicholas M. Boffi, and Eric Vanden-Eijnden. Stochastic Interpolants: A Unifying Framework for Flows and Diffusions, March 2023. URL http://arxiv.org/abs/2303.08797. arXiv:2303.08797 [cond-mat].

[3] Brandon Amos, Lei Xu, and J. Zico Kolter. Input Convex Neural Networks. In *Proceedings of the 34th International Conference on Machine Learning*, pages 146–155. PMLR, July 2017. URL https://proceedings.mlr.press/v70/amos17b.html. ISSN: 2640-3498.

[4] Jean-David Benamou and Yann Brenier. A computational fluid mechanics solution to the Monge-Kantorovich mass transfer problem. *Numerische Mathematik*, 84(3):375–393, January 2000. ISSN 0945-3245. doi: 10.1007/s002110050002. URL https://doi.org/10.1007/s002110050002.

[5] Jean-David Benamou and Guillaume Carlier. Augmented Lagrangian Methods for Transport Optimization, Mean Field Games and Degenerate Elliptic Equations. *Journal of Optimization Theory and Applications*, 167(1):1–26, October 2015. ISSN 0022-3239, 1573-2878. doi: 10.1007/s10957-015-0725-9. URL http://link.springer.com/10.1007/s10957-015-0725-9.

[6] Joe Benton, George Deligiannidis, and Arnaud Doucet. Error bounds for flow matching methods. *Transactions on Machine Learning Research*, 2024. ISSN 2835-8856. URL https://openreview.net/forum?id=uqQPyWFDhY.

[7] E. H. Brown and John W. Milnor. Topology from the Differentiable Viewpoint. *The American Mathematical Monthly*, 74(4):461, April 1967. ISSN 00029890. doi: 10.2307/2314613. URL https://www.jstor.org/stable/2314613?origin=crossref.

[8] Charlotte Bunne, Ya-Ping Hsieh, Marco Cuturi, and Andreas Krause. The Schrödinger Bridge between Gaussian Measures has a Closed Form. In *Proceedings of The 26th International Conference on Artificial Intelligence and Statistics*, pages 5802–5833. PMLR, April 2023. URL https://proceedings.mlr.press/v206/bunne23a.html. ISSN: 2640-3498.

[9] Tian Qi Chen, Yulia Rubanova, Jesse Bettencourt, and David K Duvenaud. Neural Ordinary Differential Equations.

[10] Tianrong Chen, Guan-Horng Liu, Molei Tao, and Evangelos Theodorou. Deep Momentum Multi-Marginal Schrödinger Bridge. November 2023. URL https://openreview.net/forum?id=ykvvv0gc4R.

[11] Yongxin Chen, Tryphon T. Georgiou, and Michele Pavon. On the Relation Between Optimal Transport and Schrödinger Bridges: A Stochastic Control Viewpoint. *Journal of Optimization Theory and Applications*, 169(2):671–691, May 2016. ISSN 1573-2878. doi: 10.1007/s10957-015-0803-z. URL https://doi.org/10.1007/s10957-015-0803-z.

[12] Rémi Flamary, Nicolas Courty, Alexandre Gramfort, Mokhtar Z. Alaya, Aurélie Boisbunon, Stanislas Chambon, Laetitia Chapel, Adrien Corenflos, Kilian Fatras, Nemo Fournier, Léo Gautheron, Nathalie T. H. Gayraud, Hicham Janati, Alain Rakotomamonjy, Ievgen Redko, Antoine Rolet, Antony Schutz, Vivien Seguy, Danica J. Sutherland, Romain Tavenard, Alexander Tong, and Titouan Vayer. POT: Python Optimal Transport. *Journal of Machine Learning Research*, 22(78):1–8, 2021. ISSN 1533-7928. URL http://jmlr.org/papers/v22/20-451.html.

[13] Han Huang, Jiajia Yu, Jie Chen, and Rongjie Lai. Bridging mean-field games and normalizing flows with trajectory regularization. *Journal of Computational Physics*, 487:112155, August 2023. ISSN 0021-9991. doi: 10.1016/j.jcp.2023.112155. URL https://www.sciencedirect.com/science/article/pii/S0021999123002504.

[14] Matt Jacobs, Flavien Léger, Wuchen Li, and Stanley Osher. Solving Large-Scale Optimization Problems with a Convergence Rate Independent of Grid Size. *SIAM Journal on Numerical Analysis*, 57(3):1100–1123, January 2019. ISSN 0036-1429, 1095-7170. doi: 10.1137/18M118640X. URL https://epubs.siam.org/doi/10.1137/18M118640X.

[15] Yijie Jin, Shu Liu, Hao Wu, Xiaojing Ye, and Haomin Zhou. Parameterized Wasserstein gradient flow. *Journal of Computational Physics*, 524:113660, March 2025. ISSN 0021-9991. doi: 10.1016/j.jcp.2024.113660. URL https://www.sciencedirect.com/science/article/pii/S0021999124009082.

[16] Wuchen Li and Stanley Osher. Constrained dynamical optimal transport and its Lagrangian formulation, September 2018. URL http://arxiv.org/abs/1807.00937. arXiv:1807.00937 [math].

[17] Alex Tong Lin, Samy Wu Fung, Wuchen Li, Levon Nurbekyan, and Stanley J. Osher. Alternating the population and control neural networks to solve high-dimensional stochastic mean-field games. *Proceedings of the National Academy of Sciences*, 118(31):e2024713118, August 2021. doi: 10.1073/pnas.2024713118. URL https://www.pnas.org/doi/10.1073/pnas.2024713118. Publisher: Proceedings of the National Academy of Sciences.

[18] Yaron Lipman, Ricky T. Q. Chen, Heli Ben-Hamu, Maximilian Nickel, and Matthew Le. Flow Matching for Generative Modeling. September 2022. URL https://openreview.net/forum?id=PqvMRDCJT9t.

[19] Guan-Horng Liu, Tianrong Chen, Oswin So, and Evangelos Theodorou. Deep Generalized Schrödinger Bridge. October 2022. URL https://openreview.net/forum?id=fp33Nsh0O5.

[20] Guan-Horng Liu, Yaron Lipman, Maximilian Nickel, Brian Karrer, Evangelos A. Theodorou, and Ricky T. Q. Chen. Generalized Schrödinger Bridge Matching. arXiv, April 2024. URL http://arxiv.org/abs/2310.02233. arXiv:2310.02233.

[21] Shu Liu, Wuchen Li, Hongyuan Zha, and Haomin Zhou. Neural Parametric Fokker–Planck Equation. *SIAM Journal on Numerical Analysis*, 60(3):1385–1449, June 2022. ISSN 0036-1429. doi: 10.1137/20M1344986. URL https://epubs.siam.org/doi/10.1137/20M1344986. Publisher: Society for Industrial and Applied Mathematics.

[22] Shu Liu, Stanley Osher, and Wuchen Li. A Natural Primal-Dual Hybrid Gradient Method for Adversarial Neural Network Training on Solving Partial Differential Equations, December 2024. URL http://arxiv.org/abs/2411.06278. arXiv:2411.06278 [math].

[23] Flavien Léger and Wuchen Li. Hopf-Cole transformation via generalized Schr\"odinger bridge problem, January 2019. URL http://arxiv.org/abs/1901.09051. arXiv:1901.09051 [math].

[24] Toshio Mikami. Stochastic optimal transport revisited. *SN Partial Differential Equations and Applications*, 2(1):5, February 2021. ISSN 2662-2963, 2662-2971. doi: 10.1007/s42985-020-00059-3. URL http://arxiv.org/abs/2003.11811. arXiv:2003.11811 [math].

[25] Derek Onken, Samy Wu Fung, Xingjian Li, and Lars Ruthotto. OT-Flow: Fast and Accurate Continuous Normalizing Flows via Optimal Transport. *Proceedings of the AAAI Conference on Artificial Intelligence*, 35(10):9223–9232, May 2021. ISSN 2374-3468. doi: 10.1609/aaai.v35i10.17113. URL https://ojs.aaai.org/index.php/AAAI/article/view/17113. Number: 10.

[26] Adam Paszke, Sam Gross, Francisco Massa, Adam Lerer, James Bradbury, Gregory Chanan, Trevor Killeen, Zeming Lin, Natalia Gimelshein, Luca Antiga, Alban Desmaison, Andreas Köpf, Edward Yang, Zach DeVito, Martin Raison, Alykhan Tejani, Sasank Chilamkurthy, Benoit Steiner, Lu Fang, Junjie Bai, and Soumith Chintala. PyTorch: An Imperative Style, High-Performance Deep Learning Library, December 2019. URL http://arxiv.org/abs/1912.01703. arXiv:1912.01703 [cs].

[27] Gabriel Peyré and Marco Cuturi. Computational optimal transport: With applications to data science. *Foundations and Trends® in Machine Learning*, 11(5-6):355–607, 2019. ISSN 1935-8237. doi: 10.1561/2200000073. URL http://dx.doi.org/10.1561/2200000073.

[28] Michael Poli, Stefano Massaroli, Atsushi Yamashita, Hajime Asama, Jinkyoo Park, and Stefano Ermon. Torchdyn: Implicit models and neural numerical methods in pytorch.

[29] Aram-Alexandre Pooladian, Carles Domingo-Enrich, Ricky T. Q. Chen, and Brandon Amos. Neural Optimal Transport with Lagrangian Costs. June 2024. URL https://openreview.net/forum?id=x4paJ2sJyZ.

[30] Simon Schweighofer, David Garcia, and Frank Schweitzer. An agent-based model of multi-dimensional opinion dynamics and opinion alignment. *Chaos: An Interdisciplinary Journal of Nonlinear Science*, 30(9):093139, September 2020. ISSN 1054-1500. doi: 10.1063/5.0007523. URL https://doi.org/10.1063/5.0007523.

[31] Alexander Tong, Nikolay Malkin, Guillaume Huguet, Yanlei Zhang, Jarrid Rector-Brooks, Kilian Fatras, Guy Wolf, and Yoshua Bengio. Improving and generalizing flow-based generative models with minibatch optimal transport, October 2023. URL http://arxiv.org/abs/2302.00482. arXiv:2302.00482 [cs].

[32] Cédric Villani. *Optimal Transport*, volume 338 of *Grundlehren der mathematischen Wissenschaften*. Springer, Berlin, Heidelberg, 2009. ISBN 978-3-540-71049-3 978-3-540-71050-9. doi: 10.1007/978-3-540-71050-9. URL http://link.springer.com/10.1007/978-3-540-71050-9.

[33] Hao Wu, Shu Liu, Xiaojing Ye, and Haomin Zhou. Parameterized Wasserstein Hamiltonian Flow. *SIAM Journal on Numerical Analysis*, 63(1):360–395, February 2025. ISSN 0036-1429, 1095-7170. doi: 10.1137/23M159281X. URL https://epubs.siam.org/doi/10.1137/23M159281X.

[34] Yujia Xie, Minshuo Chen, Haoming Jiang, Tuo Zhao, and Hongyuan Zha. On Scalable and Efficient Computation of Large Scale Optimal Transport. April 2019. URL https://openreview.net/forum?id=S1xA7ILFOV.

[35] Mo Zhou, Stanley Osher, and Wuchen Li. Score-based Neural Ordinary Differential Equations for Computing Mean Field Control Problems, January 2025. URL http://arxiv.org/abs/2409.16471. arXiv:2409.16471 [math].

NeurIPS Paper Checklist

1. **Claims**

   Question: Do the main claims made in the abstract and introduction accurately reflect the paper's contributions and scope?

   Answer: [Yes]

   Justification: We provide the proof of the consistency of our static formulation of the dynamic problem. We show that in all the examples of the paper 3-5 control points are enough to obtain state-of-the-art results. We further provide an ablation study on the influence of the number of control points.

   Guidelines:

   - The answer NA means that the abstract and introduction do not include the claims made in the paper.
   - The abstract and/or introduction should clearly state the claims made, including the contributions made in the paper and important assumptions and limitations. A No or NA answer to this question will not be perceived well by the reviewers.
   - The claims made should match theoretical and experimental results, and reflect how much the results can be expected to generalize to other settings.
   - It is fine to include aspirational goals as motivation as long as it is clear that these goals are not attained by the paper.

2. **Limitations**

   Question: Does the paper discuss the limitations of the work performed by the authors?

   Answer: [Yes]

   Justification: In Sections section 5 we discuss the algorithm's computational complexity and its limitation for high-dimensional SOC problems. We further discuss, see Section 6, the algorithm's current limitation on using MLPs for the NODE architecture.

   Guidelines:

   - The answer NA means that the paper has no limitation while the answer No means that the paper has limitations, but those are not discussed in the paper.
   - The authors are encouraged to create a separate "Limitations" section in their paper.
   - The paper should point out any strong assumptions and how robust the results are to violations of these assumptions (e.g., independence assumptions, noiseless settings, model well-specification, asymptotic approximations only holding locally). The authors should reflect on how these assumptions might be violated in practice and what the implications would be.
   - The authors should reflect on the scope of the claims made, e.g., if the approach was only tested on a few datasets or with a few runs. In general, empirical results often depend on implicit assumptions, which should be articulated.
   - The authors should reflect on the factors that influence the performance of the approach. For example, a facial recognition algorithm may perform poorly when image resolution is low or images are taken in low lighting. Or a speech-to-text system might not be used reliably to provide closed captions for online lectures because it fails to handle technical jargon.
   - The authors should discuss the computational efficiency of the proposed algorithms and how they scale with dataset size.
   - If applicable, the authors should discuss possible limitations of their approach to address problems of privacy and fairness.
   - While the authors might fear that complete honesty about limitations might be used by reviewers as grounds for rejection, a worse outcome might be that reviewers discover limitations that aren't acknowledged in the paper. The authors should use their best judgment and recognize that individual actions in favor of transparency play an important role in developing norms that preserve the integrity of the community. Reviewers will be specifically instructed to not penalize honesty concerning limitations.

3. **Theory Assumptions and Proofs**

Question: For each theoretical result, does the paper provide the full set of assumptions and a complete (and correct) proof?

Answer: [Yes]

Justification: All the hypothesis and proofs for Theorem 1 and Theorem 2 are clearly stated in the Appendix.

Guidelines:

- The answer NA means that the paper does not include theoretical results.
- All the theorems, formulas, and proofs in the paper should be numbered and cross-referenced.
- All assumptions should be clearly stated or referenced in the statement of any theorems.
- The proofs can either appear in the main paper or the supplemental material, but if they appear in the supplemental material, the authors are encouraged to provide a short proof sketch to provide intuition.
- Inversely, any informal proof provided in the core of the paper should be complemented by formal proofs provided in appendix or supplemental material.
- Theorems and Lemmas that the proof relies upon should be properly referenced.

4. **Experimental Result Reproducibility**

Question: Does the paper fully disclose all the information needed to reproduce the main experimental results of the paper to the extent that it affects the main claims and/or conclusions of the paper (regardless of whether the code and data are provided or not)?

Answer: [Yes]

Justification: All the necessary information is in Table 4

Guidelines:

- The answer NA means that the paper does not include experiments.
- If the paper includes experiments, a No answer to this question will not be perceived well by the reviewers: Making the paper reproducible is important, regardless of whether the code and data are provided or not.
- If the contribution is a dataset and/or model, the authors should describe the steps taken to make their results reproducible or verifiable.
- Depending on the contribution, reproducibility can be accomplished in various ways. For example, if the contribution is a novel architecture, describing the architecture fully might suffice, or if the contribution is a specific model and empirical evaluation, it may be necessary to either make it possible for others to replicate the model with the same dataset, or provide access to the model. In general. releasing code and data is often one good way to accomplish this, but reproducibility can also be provided via detailed instructions for how to replicate the results, access to a hosted model (e.g., in the case of a large language model), releasing of a model checkpoint, or other means that are appropriate to the research performed.
- While NeurIPS does not require releasing code, the conference does require all submissions to provide some reasonable avenue for reproducibility, which may depend on the nature of the contribution. For example
  (a) If the contribution is primarily a new algorithm, the paper should make it clear how to reproduce that algorithm.
  (b) If the contribution is primarily a new model architecture, the paper should describe the architecture clearly and fully.
  (c) If the contribution is a new model (e.g., a large language model), then there should either be a way to access this model for reproducing the results or a way to reproduce the model (e.g., with an open-source dataset or instructions for how to construct the dataset).
  (d) We recognize that reproducibility may be tricky in some cases, in which case authors are welcome to describe the particular way they provide for reproducibility. In the case of closed-source models, it may be that access to the model is limited in some way (e.g., to registered users), but it should be possible for other researchers to have some path to reproducing or verifying the results.

5. **Open access to data and code**

   Question: Does the paper provide open access to the data and code, with sufficient instructions to faithfully reproduce the main experimental results, as described in supplemental material?

   Answer: [Yes]

   Justification: We provide a copy of our code in the supplemental materials.

   Guidelines:

   - The answer NA means that paper does not include experiments requiring code.
   - Please see the NeurIPS code and data submission guidelines (`https://nips.cc/public/guides/CodeSubmissionPolicy`) for more details.
   - While we encourage the release of code and data, we understand that this might not be possible, so "No" is an acceptable answer. Papers cannot be rejected simply for not including code, unless this is central to the contribution (e.g., for a new open-source benchmark).
   - The instructions should contain the exact command and environment needed to run to reproduce the results. See the NeurIPS code and data submission guidelines (`https://nips.cc/public/guides/CodeSubmissionPolicy`) for more details.
   - The authors should provide instructions on data access and preparation, including how to access the raw data, preprocessed data, intermediate data, and generated data, etc.
   - The authors should provide scripts to reproduce all experimental results for the new proposed method and baselines. If only a subset of experiments are reproducible, they should state which ones are omitted from the script and why.
   - At submission time, to preserve anonymity, the authors should release anonymized versions (if applicable).
   - Providing as much information as possible in supplemental material (appended to the paper) is recommended, but including URLs to data and code is permitted.

6. **Experimental Setting/Details**

   Question: Does the paper specify all the training and test details (e.g., data splits, hyperparameters, how they were chosen, type of optimizer, etc.) necessary to understand the results?

   Answer: [Yes]

   Justification: See Table 4

   Guidelines:

   - The answer NA means that the paper does not include experiments.
   - The experimental setting should be presented in the core of the paper to a level of detail that is necessary to appreciate the results and make sense of them.
   - The full details can be provided either with the code, in appendix, or as supplemental material.

7. **Experiment Statistical Significance**

   Question: Does the paper report error bars suitably and correctly defined or other appropriate information about the statistical significance of the experiments?

   Answer:[Yes]

   Justification: All the experiments were run with three different seeds.

   Guidelines:

   - The answer NA means that the paper does not include experiments.
   - The authors should answer "Yes" if the results are accompanied by error bars, confidence intervals, or statistical significance tests, at least for the experiments that support the main claims of the paper.
   - The factors of variability that the error bars are capturing should be clearly stated (for example, train/test split, initialization, random drawing of some parameter, or overall run with given experimental conditions).

- The method for calculating the error bars should be explained (closed form formula, call to a library function, bootstrap, etc.)
- The assumptions made should be given (e.g., Normally distributed errors).
- It should be clear whether the error bar is the standard deviation or the standard error of the mean.
- It is OK to report 1-sigma error bars, but one should state it. The authors should preferably report a 2-sigma error bar than state that they have a 96% CI, if the hypothesis of Normality of errors is not verified.
- For asymmetric distributions, the authors should be careful not to show in tables or figures symmetric error bars that would yield results that are out of range (e.g. negative error rates).
- If error bars are reported in tables or plots, The authors should explain in the text how they were calculated and reference the corresponding figures or tables in the text.

8. **Experiments Compute Resources**

   Question: For each experiment, does the paper provide sufficient information on the computer resources (type of compute workers, memory, time of execution) needed to reproduce the experiments?

   Answer:[Yes]

   Justification: In Section 4 we specified the computational resources and the time was reported in Table 1.

   Guidelines:

   - The answer NA means that the paper does not include experiments.
   - The paper should indicate the type of compute workers CPU or GPU, internal cluster, or cloud provider, including relevant memory and storage.
   - The paper should provide the amount of compute required for each of the individual experimental runs as well as estimate the total compute.
   - The paper should disclose whether the full research project required more compute than the experiments reported in the paper (e.g., preliminary or failed experiments that didn't make it into the paper).

9. **Code Of Ethics**

   Question: Does the research conducted in the paper conform, in every respect, with the NeurIPS Code of Ethics `https://neurips.cc/public/EthicsGuidelines`?

   Answer: [Yes]

   Justification: We have reviewed the NeurIPS Code of Ethics and ensured that our research satisfies it.

   Guidelines:

   - The answer NA means that the authors have not reviewed the NeurIPS Code of Ethics.
   - If the authors answer No, they should explain the special circumstances that require a deviation from the Code of Ethics.
   - The authors should make sure to preserve anonymity (e.g., if there is a special consideration due to laws or regulations in their jurisdiction).

10. **Broader Impacts**

    Question: Does the paper discuss both potential positive societal impacts and negative societal impacts of the work performed?

    Answer: [Yes]

    Justification: We included a brief discussion on the possible use of action-minimizing solvers in the study of population dynamics.

    Guidelines:

    - The answer NA means that there is no societal impact of the work performed.
    - If the authors answer NA or No, they should explain why their work has no societal impact or why the paper does not address societal impact.

- Examples of negative societal impacts include potential malicious or unintended uses (e.g., disinformation, generating fake profiles, surveillance), fairness considerations (e.g., deployment of technologies that could make decisions that unfairly impact specific groups), privacy considerations, and security considerations.
- The conference expects that many papers will be foundational research and not tied to particular applications, let alone deployments. However, if there is a direct path to any negative applications, the authors should point it out. For example, it is legitimate to point out that an improvement in the quality of generative models could be used to generate deepfakes for disinformation. On the other hand, it is not needed to point out that a generic algorithm for optimizing neural networks could enable people to train models that generate Deepfakes faster.
- The authors should consider possible harms that could arise when the technology is being used as intended and functioning correctly, harms that could arise when the technology is being used as intended but gives incorrect results, and harms following from (intentional or unintentional) misuse of the technology.
- If there are negative societal impacts, the authors could also discuss possible mitigation strategies (e.g., gated release of models, providing defenses in addition to attacks, mechanisms for monitoring misuse, mechanisms to monitor how a system learns from feedback over time, improving the efficiency and accessibility of ML).

11. **Safeguards**

    Question: Does the paper describe safeguards that have been put in place for responsible release of data or models that have a high risk for misuse (e.g., pretrained language models, image generators, or scraped datasets)?

    Answer: [NA]

    Justification: There is no foreseeable high risk for misuse.

    Guidelines:

    - The answer NA means that the paper poses no such risks.
    - Released models that have a high risk for misuse or dual-use should be released with necessary safeguards to allow for controlled use of the model, for example by requiring that users adhere to usage guidelines or restrictions to access the model or implementing safety filters.
    - Datasets that have been scraped from the Internet could pose safety risks. The authors should describe how they avoided releasing unsafe images.
    - We recognize that providing effective safeguards is challenging, and many papers do not require this, but we encourage authors to take this into account and make a best faith effort.

12. **Licenses for existing assets**

    Question: Are the creators or original owners of assets (e.g., code, data, models), used in the paper, properly credited and are the license and terms of use explicitly mentioned and properly respected?

    Answer: [Yes]

    Justification: We provide in the Appendix F the licences and terms of the benchmark codes.

    Guidelines:

    - The answer NA means that the paper does not use existing assets.
    - The authors should cite the original paper that produced the code package or dataset.
    - The authors should state which version of the asset is used and, if possible, include a URL.
    - The name of the license (e.g., CC-BY 4.0) should be included for each asset.
    - For scraped data from a particular source (e.g., website), the copyright and terms of service of that source should be provided.
    - If assets are released, the license, copyright information, and terms of use in the package should be provided. For popular datasets, `paperswithcode.com/datasets` has curated licenses for some datasets. Their licensing guide can help determine the license of a dataset.

- For existing datasets that are re-packaged, both the original license and the license of the derived asset (if it has changed) should be provided.
- If this information is not available online, the authors are encouraged to reach out to the asset's creators.

13. **New Assets**

    Question: Are new assets introduced in the paper well documented and is the documentation provided alongside the assets?

    Answer: [Yes]

    Justification: We appropriately cited the code we used for our benchmarks.

    Guidelines:

    - The answer NA means that the paper does not release new assets.
    - Researchers should communicate the details of the dataset/code/model as part of their submissions via structured templates. This includes details about training, license, limitations, etc.
    - The paper should discuss whether and how consent was obtained from people whose asset is used.
    - At submission time, remember to anonymize your assets (if applicable). You can either create an anonymized URL or include an anonymized zip file.

14. **Crowdsourcing and Research with Human Subjects**

    Question: For crowdsourcing experiments and research with human subjects, does the paper include the full text of instructions given to participants and screenshots, if applicable, as well as details about compensation (if any)?

    Answer: [NA]

    Justification: No crowdsourcing or research with human resources.

    Guidelines:

    - The answer NA means that the paper does not involve crowdsourcing nor research with human subjects.
    - Including this information in the supplemental material is fine, but if the main contribution of the paper involves human subjects, then as much detail as possible should be included in the main paper.
    - According to the NeurIPS Code of Ethics, workers involved in data collection, curation, or other labor should be paid at least the minimum wage in the country of the data collector.

15. **Institutional Review Board (IRB) Approvals or Equivalent for Research with Human Subjects**

    Question: Does the paper describe potential risks incurred by study participants, whether such risks were disclosed to the subjects, and whether Institutional Review Board (IRB) approvals (or an equivalent approval/review based on the requirements of your country or institution) were obtained?

    Answer: [NA]

    Justification: No participants used.

    Guidelines:

    - The answer NA means that the paper does not involve crowdsourcing nor research with human subjects.
    - Depending on the country in which research is conducted, IRB approval (or equivalent) may be required for any human subjects research. If you obtained IRB approval, you should clearly state this in the paper.
    - We recognize that the procedures for this may vary significantly between institutions and locations, and we expect authors to adhere to the NeurIPS Code of Ethics and the guidelines for their institution.
    - For initial submissions, do not include any information that would break anonymity (if applicable), such as the institution conducting the review.

16. **Declaration of LLM usage**

Question: Does the paper describe the usage of LLMs if it is an important, original, or non-standard component of the core methods in this research? Note that if the LLM is used only for writing, editing, or formatting purposes and does not impact the core methodology, scientific rigorousness, or originality of the research, declaration is not required.

Answer:[NA]

Justification: Our research does not involve LLMs.

Guidelines:

- The answer NA means that the core method development in this research does not involve LLMs as any important, original, or non-standard components.
- Please refer to our LLM policy (`https://neurips.cc/Conferences/2025/LLM`) for what should or should not be described.

A Deterministic and SOC problems

We now show the equivalence of

$$\begin{aligned} &\inf_{\rho,v} \int_0^1 \int_{\mathbb{R}^d} \frac{1}{2}\|v(t,x)\|^2 \rho(t,x)dx + F(\rho(t)) + \mathcal{FI}(\rho(t))\, dt \\ &\quad \text{subject to} \quad \partial_t \rho + \nabla \cdot (\rho v) = 0, \quad \rho(0,\cdot) = \rho_0, \quad \rho(1,\cdot) = \rho_1, \end{aligned} \tag{17}$$

and

$$\begin{aligned} &\inf_{\rho(t,x),u(t,x)} \int_0^1 \int_{\mathbb{R}^d} \frac{1}{2}\|u(t,x)\|^2 \rho(t,x)dx + F(\rho(t))\, dt \\ &\quad \text{subject to} \quad \partial_t \rho + \nabla \cdot (\rho u) = \frac{\sigma^2}{2}\Delta\rho, \quad \rho(0,\cdot) = \rho_0, \quad \rho(1,\cdot) = \rho_1. \end{aligned} \tag{18}$$

Proof. In what follows, we use the notation δ_ρ for the L^2 gradient.

Let S be a Lagrange multiplier for (17), then KKT conditions for (17) are given by

$$\begin{aligned} v = \nabla S \quad \rho, \text{ a.e.} \\ \partial_t S + \frac{1}{2}\|\nabla S\|^2 = -\delta_\rho F(\rho) - \delta_\rho \mathcal{FI}(\rho), \\ \partial_t \rho + \nabla \cdot (\rho v) = 0. \end{aligned}$$

Define $\Phi = S + \sigma^2/2 \log \rho$, and $u := \nabla\Phi$, ρ a.e. Then the pair (ρ, u) satisfies

$$\begin{aligned} u = \nabla\Phi, \quad \rho \text{ a.e.} \\ \partial_t \Phi + \frac{1}{2}\|\nabla\Phi\|^2 = -\delta_\rho F(\rho), \\ \partial_t \rho + \nabla \cdot (\rho u) = \frac{\sigma^2}{2}\Delta\rho, \end{aligned}$$

which is in turn the KKT conditions of the optimization problem (18). □

B Equivalence of dynamic and static frameworks

Here we show the equivalence between

$$\begin{aligned} &\inf_{\rho,v} \int_0^1 \int_{\mathbb{R}^d} \frac{1}{2}\|v(t,x)\|^2 \rho(t,x)dx + F(\rho(t))\, dt \\ &\quad \text{subject to} \quad \partial_t \rho + \nabla \cdot (\rho v) = 0, \quad \rho(0,\cdot) = \rho_0, \quad \rho(1,\cdot) = \rho_1, \end{aligned}$$

and

$$\inf_{\pi \in \tilde{\Pi}(\rho_0,\rho_1)} c(\pi) = \inf_{\pi \in \tilde{\Pi}(\rho_0,\rho_1)} \inf_{\gamma \in \Gamma(\pi)} \mathcal{A}(\gamma).$$

Proof. Observe that a local minimizer of (6) (ρ, v) defines a C^1-diffeomorphic curve $\gamma_{\rho,v}$ as the flow

$$\gamma(t,x) = x + \int_0^t v(s,\gamma(s,x))ds,$$

and the coupling $\pi_{\rho,v} = (x, \gamma(1,x))$. The coupling $\pi_{\rho,v}$ and path $\gamma_{\rho,v}$ are an admissible pair for (11). From the definition of $\gamma_{\rho,v}$, it follows that $\rho_{\gamma_{\rho,\nu}(t)} = (\gamma_{\rho,\nu}(t))_\#(\rho_0) = \rho$, and

$$\int_0^1 \int_{\mathbb{R}^d} \frac{1}{2}\|v(t,x)\|^2 \rho(t,x)dxdt = \mathcal{A}(\gamma_{\rho,v}),$$

then

$$\int_0^1 \int_{\mathbb{R}^d} \frac{1}{2}\|v(t,x)\|^2 \rho(t,x)dx + F(\rho)\, dt = \mathcal{A}(\gamma_{\rho,v}) + \int_0^1 F(\rho_{\gamma,v})dt.$$

Thus (6) upper bounds (11). Now, given a local minimizer of (11) (π, γ), the density $\rho_{\pi,\gamma}(t,\cdot) = (\gamma_t(\cdot))_{\#}(\rho_0)$ and the velocity field

$$v(t, \gamma(t,x)) = \frac{d}{dt}\gamma(t,x), \quad \gamma(0,x) = x \sim \rho_0,$$

define an admissible pair of (6). As before,

$$\mathcal{A}(\gamma) + \int_0^1 F(\rho_\gamma)dt = \int_0^1 \int_{\mathbb{R}^d} \frac{1}{2}\|v_{\pi,\gamma}(t,x)\|^2 \rho_{\pi,\gamma}(t,x)dx + F(\rho_{\pi,\gamma})dt.$$

Thus, (11) upper bounds (6). □

C Wasserstein error bounds for interpolation

Theorem 3. *Assume that T is Lipschitz in its second variable with a constant C, in the sense, $\forall z \in \mathbb{R}^d$ and any $\theta, \tilde{\theta} \in \mathbb{R}^D$,*

$$\|T(z,\theta) - T(z,\tilde{\theta})\| \leq C\|\theta - \tilde{\theta}\|,$$

then

$$W_2(\rho_\theta, \rho_{\tilde{\theta}}) \leq C\|\theta - \tilde{\theta}\|. \tag{19}$$

Proof. From the static definition of the Wasserstein distance Equation (3), we have

$$W_2(\rho_\theta, \rho_{\tilde{\theta}}) \leq \left(\int_{\mathbb{R}^d} \|T(z,\theta) - T(z,\tilde{\theta})\|^2 \lambda(z)dz\right)^{1/2} \leq C||\theta - \tilde{\theta}\|.$$

□

We recognize that T being Lipschitz in the above sense is strong. We leave for future research, relaxing it to locally Lipschitz, a more feasible condition.

Corollary 1. *Let $\theta_{0\to1}$ and $\tilde{\theta}_{0\to1}$ denote two curves in the parameter space. Following the hypothesis on Theorem 3, it follows that $\forall t \in [0,1]$*

$$W_2(\rho_{\theta(t)}, \rho_{\tilde{\theta}(t)}) \leq C||\theta(t) - \tilde{\theta}(t)\|.$$

Corollary 2. *Let $\theta_{0\to1}$ be a curve in parameter space with continuous derivatives up to order $l \geq 1$, and let $\tilde{\theta}_{0\to1}$ be the piecewise cubic Hermite spline interpolation of $\theta(t)$ at K uniformly spaced points $\{t_i = \frac{i}{K+1}\}_{i=0}^{K+1}$. Define $\kappa := \min(l, 4)$, then*

$$\|\theta_{0\to1} - \tilde{\theta}_{0\to1}\| \leq M_\kappa \max_{\xi\in[0,1]} \|\theta^{(\kappa)}(\xi)\|\, h^\kappa,$$

where $h = \frac{1}{K+1}$ and M_κ is a constant depending on κ. With $\theta^{(\kappa)}$, the κ derivative of the path $\theta(t)$. Furthermore for all $t \in [0,1]$, the Wasserstein distance between the density paths at time t is given by

$$W_2(\rho_{\theta(t)}, \rho_{\tilde{\theta}(t)}) \leq CM_\kappa \max_{\xi\in[0,1]} \|\theta^{(\kappa)}(\xi)\|\, h^\kappa,$$

where C is the Lipschitz constant from Theorem 3.

Theorem 4. *Let $\theta_{0\to1}$ be a curve in parameter space with continuous derivatives up to order $l \geq 2$, and let $\tilde{\theta}_{0\to1}$ be the cubic Hermite spline interpolation of $\theta(t)$ at K uniformly spaced points $\{t_i = \frac{i}{K+1}\}_{i=0}^{K+1}$. Define $\kappa := \min(l, 4)$.*

Assume that:

1. *F is Lipschitz with respect to the Wasserstein-2 distance with constant M_F.*
2. *$\|\partial_\theta T(z,\theta)\| < M_{\partial_\theta T}$, for some constant $M_{\partial_\theta T}$ for all z and θ.*
3. *$\partial_\theta T(z,\theta)$ is Lipschitz continuous in θ for all z with Lipschitz constant C_{∂_θ}.*

4. $\|\theta'(t)\| < M_{\theta'}$, *for some constant* $M_{\partial_{\theta'}}$ *for all* $t \in [0,1]$.

Then the error in the action functional is bounded by:

$$|A[\theta_{0\to 1}] - A[\tilde{\theta}_{0\to 1}]| \le C_{\mathcal{A}} \max_{\xi\in[0,1]} \|\theta^{(\kappa)}(\xi)\|\, h^{\kappa-1},$$

where $h = \frac{1}{K+1}$ *and* $C_{\mathcal{A}}$ *is defined below at the end of the proof.*

Proof. We split the proof into two parts, one part on a bound for the kinetic energy term, and the other on a bound for the potential energy term. The bound for the potential energy follows from the Lipschitz continuity of F and Corollary 1

$$\int_0^1 |F(\rho_{\theta(t)}) - F(\rho_{\tilde{\theta}(t)})|dt \le \int_0^1 M_F W_2(\rho_{\theta(t)}, \rho_{\tilde{\theta}(t)})dt \le M_F M_\kappa \cdot h^\kappa \max_{\xi\in[0,1]} \|\theta^{(\kappa)}(\xi)\|.$$

The bound for the kinetic energy can be derived by assumptions 2–4 as

$$\begin{aligned}
&\int_0^1 \Big|\mathbb{E}_{z\sim\lambda}\Big\|\frac{d}{dt}x_{\theta(t)}(z)\Big\|^2 - \mathbb{E}_{z\sim\lambda}\Big\|\frac{d}{dt}x_{\tilde{\theta}(t)}(z)\Big\|^2\Big|dt\\
&\le \int_0^1 \mathbb{E}_{z\sim\lambda}\Big|\Big\|\frac{d}{dt}x_{\theta(t)}(z)\Big\|^2 - \Big\|\frac{d}{dt}x_{\tilde{\theta}(t)}(z)\Big\|^2\Big|dt\\
&\le \int_0^1 \mathbb{E}_{z\sim\lambda}\Big[\Big(\Big\|\frac{d}{dt}x_{\theta(t)}(z)\Big\| + \Big\|\frac{d}{dt}x_{\tilde{\theta}(t)}(z)\Big\|\Big)\Big\|\frac{d}{dt}x_{\theta(t)}(z) - \frac{d}{dt}x_{\tilde{\theta}(t)}(z)\Big\|\Big]dt\\
&\le \int_0^1 \mathbb{E}_{z\sim\lambda}\Big[\Big(\|(\partial_\theta T)(z,\theta(t))\|\|\theta'(t)\| + \|(\partial_\theta T)(z,\tilde{\theta}(t))\|\|\tilde{\theta}'(t)\|\Big)\\
&\qquad\cdot \|(\partial_\theta T)(z,\theta(t))\theta'(t) - (\partial_\theta T)(z,\tilde{\theta}(t))\tilde{\theta}'(t)\|\Big]dt\\
&\le (M_{\partial_\theta T}M_{\theta'} + M_{\partial_\theta T}M_{\tilde{\theta}'})\int_0^1 \mathbb{E}_{z\sim\lambda}\|(\partial_\theta T)(z,\theta(t))\theta'(t) - (\partial_\theta T)(z,\tilde{\theta}(t))\tilde{\theta}'(t)\|dt\\
&= M_{\partial_\theta T}(M_{\theta'} + M_{\tilde{\theta}'})\int_0^1 \mathbb{E}_{z\sim\lambda}\|(\partial_\theta T)(z,\theta(t))\theta'(t) - (\partial_\theta T)(z,\tilde{\theta}(t))\tilde{\theta}'(t)\|dt\\
&\le M_{\partial_\theta T}(M_{\theta'} + M_{\tilde{\theta}'})\int_0^1 \mathbb{E}_{z\sim\lambda}\Big[\|(\partial_\theta T)(z,\theta(t))\theta'(t) - (\partial_\theta T)(z,\theta(t))\tilde{\theta}'(t)\|\\
&\qquad + \|(\partial_\theta T)(z,\theta(t))\tilde{\theta}'(t) - (\partial_\theta T)(z,\tilde{\theta}(t))\tilde{\theta}'(t)\|\Big]dt\\
&\le M_{\partial_\theta T}(M_{\theta'} + M_{\tilde{\theta}'})\int_0^1 \mathbb{E}_{z\sim\lambda}\Big[\|(\partial_\theta T)(z,\theta(t))\|\|\theta'(t) - \tilde{\theta}'(t)\|\\
&\qquad + \|(\partial_\theta T)(z,\theta(t)) - (\partial_\theta T)(z,\tilde{\theta}(t))\|\|\tilde{\theta}'(t)\|\Big]dt\\
&\le M_{\partial_\theta T}(M_{\theta'} + M_{\tilde{\theta}'})\int_0^1 \Big(M_{\partial_\theta T}\|\theta'(t) - \tilde{\theta}'(t)\| + C_{\partial_\theta}\|\theta(t) - \tilde{\theta}(t)\|\|\tilde{\theta}'(t)\|\Big)\,dt\\
&\le M_{\partial_\theta T}(M_{\theta'} + M_{\tilde{\theta}'})\left(M_{\partial_\theta T}M_{\kappa-1}h^{\kappa-1} + C_{\partial_\theta}M_\kappa h^\kappa M_{\tilde{\theta}'}\right)\max_{\xi\in[0,1]}\|\theta^{(\kappa)}(\xi)\|.
\end{aligned}$$

A combination of the above two bounds concludes with

$$C_{\mathcal{A}} = \max\{M_F M_\kappa h, M_{\partial_\theta T}(M_{\theta'} + M_{\tilde{\theta}'})(M_{\partial_\theta T}M_{\kappa-1} + C_{\partial_\theta}M_\kappa M_{\tilde{\theta}'}h)\}.$$

□

We recognize that hypothesis 1 on Theorem 4, which requires F to be Lipschitz with respect to the W_2 metric, is a strong assumption for general functionals F. When F consists of linear potentials and bilinear interaction potentials whose corresponding $V(x)$ and $W(x-y)$ are Lipschitz continuous with constants M_V and M_W, the functional $F(\rho) = \int_{\mathbb{R}^d} V(x)\rho(x)dx + \int_{\mathbb{R}^d\times\mathbb{R}^d} W(x-y)\rho(x)\rho(y)dxdy$

is also Lipschitz. To show this, let $\mu, \nu \in \mathcal{P}(\mathbb{R}^d)$ and $T_{\mu\to\nu}$ denote the Monge map between them, then

$$
\begin{aligned}
&|F(\mu) - F(\nu)| = \\
&= |\mathbb{E}_{X\sim\mu}[V(X)] + \mathbb{E}_{X\sim\mu}\mathbb{E}_{Y\sim\mu}[W(X-Y)] - (\mathbb{E}_{X\sim\nu}[V(X)] + \mathbb{E}_{X\sim\nu}\mathbb{E}_{Y\sim\nu}[W(X-Y)])\,| \\
&\leq \mathbb{E}_{X\sim\mu}|V(X) - V(T_{\mu\to\nu}(X))| + \mathbb{E}_{X\sim\mu}\mathbb{E}_{Y\sim\mu}|W(X-Y) - W(T_{\mu\to\nu}(X) - T_{\mu\to\nu}(Y))| \\
&\leq (M_V + 2M_W)W_2(\mu,\nu).
\end{aligned}
$$

Observe that the last inequality follows from using the Lipschitz condition on V and W, and the following application of Hölder inequality,

$$
\mathbb{E}_{X\sim\mu}[|X - T_{\mu\to\nu}(X)|] \leq (\mathbb{E}_{X\sim\mu}[|X - T_{\mu\to\nu}(X)|^2])^{1/2}(\mathbb{E}_{X\sim\mu}[1^2])^{1/2} = (\mathbb{E}_{X\sim\mu}[|X - T_{\mu\to\nu}(X)|^2])^{1/2}.
$$

D NODEs

See [9] for the standard reference on NODEs. For the NODE

$$
\frac{d\psi(\tau,z)}{d\tau} = v_\theta(\tau, \psi(\tau,z)), \quad \psi(0,z) = z \sim \lambda,
$$

initialized at $\rho(0,z) \sim \mathcal{N}(0,I)$, let $\rho(\tau,\cdot) := \psi(\tau,\cdot)_\#\lambda$, then

$$
\frac{d}{d\tau}\log(\rho(\tau,x))|_{x=\psi(\tau,z)} = -\nabla\cdot v_\theta(\tau,\psi(\tau,z))), \tag{20}
$$

and

$$
\begin{aligned}
\frac{d(\nabla_x \log\rho(\tau,x))}{d\tau}|_{x=\psi(\tau,z)} &= -\nabla(\nabla\cdot v_\theta(\tau,\psi(\tau,z))) \\
&\quad - (\nabla v_\theta(\tau,\psi(\tau,z)))^T \nabla_x \log\rho(\tau,x)|_{x=\psi(\tau,z)}
\end{aligned} \tag{21}
$$

with initial conditions $\log(\rho(0,z)) = \log(\rho_{\mathcal{N}}(z))$, where $\rho_{\mathcal{N}}(z)$ is the density of a standard normal distribution, and $\nabla_x \log\rho(0,x)|_{x=z} = -z$ respectively. Although it is not necessary to use a Gaussian density for the initial condition, it is common in the literature, these quantities might not be accessible for other densities.

The result for (20) is standard and we do not include the proof here. Although Equation (21) has been proved before, see e.g., [35], we provide a proof for completeness.

Proof. For this proof, we assume $\rho(\tau,x)$ has continuous second-order derivatives with respect to τ and x. In what follows, we use the short hand notation ψ to indicate $\psi(\tau,z)$, and v instead of v_θ.

$$
\begin{aligned}
\frac{d}{d\tau}\nabla_x\log(\rho) &= \partial_\tau\nabla_x\log(\rho) + \nabla_x^2\log(\rho)\,v \\
&= \nabla_x\rho^{-1}\partial_\tau\rho + \nabla_x^2\log(\rho)\,v \\
&= -\nabla_x\rho^{-1}\nabla\cdot(\rho v) + \nabla_x^2\log(\rho)\,v \\
&= -\nabla_x(\nabla_x\log(\rho)^T v + \nabla_x\cdot v) + \nabla_x^2\log(\rho)\,v \\
&= -\nabla_x v^T\log(\rho) - \nabla_x(\nabla_x\cdot v).
\end{aligned}
$$

The first equality follows from the dynamical system $\frac{d\psi}{d\tau} = v(\tau,\psi(\tau,z))$, the third equality follows from the continuity equation $\partial_\tau\rho = -\nabla\cdot(\rho v)$, and the fourth equality from $\rho^{-1}\nabla_x\rho = \nabla_x\log(\rho)$. □

E Algorithms/Implementation details

We use two separate optimizers: one for the boundary conditions (θ_0,θ_1) (Algorithm 2) and another for the control points $\{\theta_{t_i}\}_{i=1}^K$ (Algorithm 1). We use Adam optimizers [26] in both cases. For the learning rate scheduler, we used StepLR or cosine, with specifics provided for each experiment.

A key implementation challenge is preserving PyTorch's computational graph. Specifically, the 'torch.load' operation does not retain the graph for gradient-based optimization. This is particularly

problematic in Algorithm 1, where the interpolated points $\theta(t_j)$ used in the trapezoidal integration must track the computational graph with the spline control points to enable proper gradient flow during optimization. When 'torch.load' is used to assign models, this computational graph is lost, disconnecting the density path from the control point optimization.

To address this issue, we re-implemented the MLP architecture from scratch, passing weights and biases as explicit function arguments rather than storing them as internal model parameters, see Algorithm 4. While effective, this approach introduces limitations to architectural flexibility: testing new network architectures requires either hard-coding them or developing alternative methods to preserve computational graphs when loading pre-trained models. We leave overcoming this limitation to future research.

Algorithm 1 Path optimization

Require: Parametric points $\{\theta_{t_i}\}_{i=0}^{K+1}$, potential function F, N samples$\{z_i\}_{i=1}^{M} \sim \lambda$, number of optimization steps Q_1.

Initialize spline in parameter space with $\{\theta_{t_i}\}_{i=0}^{K+1}$.
for number of iterations Q_1 **do**
    Obtain $\{\theta(t_j)\}_{j=0}^{N}$ by evaluating the current spline at time steps $t_j = \frac{j}{N}$.
    Evaluate the $N+1$ pushforwards $\{T_{\theta(t_j)}(z_i)\}_{i=0,j=1}^{N,M}$.
    if Entropy or Fisher Information **then**
        Obtain entropy Equation (20) score from (21).
    end if
    Evaluate the Equation (12) by integrating in time by trapezoidal rule and evaluating the expectations via Monte Carlo.
    Update weights $\{\theta_{t_i}\}_{i=1}^{K}$ via gradient descent.
end for
return $\{\theta_{t_i}\}_{i=1}^{K}$

Algorithm 2 Coupling optimization

Require: Sampling function from ρ_0, sampling function from ρ_1, potential function F, control points $\{\theta_{t_i}\}_{i=0}^{K+1}$, weights α_0, α_1, samples$\{z_k\}_{k=1}^{M} \sim \lambda$, number of optimization steps Q_2.

for number of iterations Q_2 **do**
    Sample M points from $\{x_0^k\}_{k=1}^{M} \sim \rho_0$, and $\{x_1^k\}_{k=1}^{M} \sim \rho_1$.
    Evaluate $\ell = \sum_{j=0}^{1} \frac{1}{M} \left[\sum_{k=1}^{M} \alpha_j L((T_{\theta_j}(z_k), x_j^k)\right]$.
    Obtain $\{\theta(t_j)\}_{j=0}^{N}$ by evaluating the current spline at time steps $t_j = \frac{j}{N}$.
    Evaluate the $N+1$ pushforwards $\{T_{\theta(t_j)}(z_k)\}_{i=0,k=1}^{N,M}$.
    if Entropy or Fisher Information **then**
        Obtain entropy Equation (20) score from (21).
    end if
    Evaluate the Equation (12) by integrating in time by trapezoidal rule and evaluating the expectations via Monte Carlo.
    Update θ_0, θ_1 by minimizing (16) via gradient descent.
end for
return θ_0, θ_1

E.1 Hyperparameter Sensitivity and Tuning

Neural ODE architecture: The neural ODE model defines the parameter space and must be sufficiently expressive to capture the boundary distributions. Key considerations:

- **Architecture sizing:** Use larger networks than minimally required for boundary fitting. For example, while a [2,64,4] architecture can learn our V-neck boundaries accurately, we needed [2,128,4] to capture the solution complexity when potential terms significantly alter the density shape.

Algorithm 3 PDPO

Require: Sampling function for ρ_0, sampling function for ρ_1, reference density λ potential function F, number of control points K, weights α_0, α_1, initialized θ_0, θ_1, number of total iterations Q, number of path optimization steps Q_1, number of coupling optimization steps Q_2, number of geodesic-warmup steps Q_3.

Initialize θ_{t_i} using an equispaced linear interpolation of θ_0 and θ_1.
Run Q_3 steps of geodesic warmup.
for number of iterations Q **do**
    Sample M points $\{z_i\}_{i=1}^M \sim \lambda$,
    Update $\{\theta_{t_i}\}_{i=1}^K$ by minimizing the action of the points $\{z_i\}_{i=1}^M$ using Algorithm 1.
    Update (θ_0, θ_1) using the points $\{z_i\}_{i=1}^M$ in Algorithm 2.
end for
return $\{\theta_{t_i}\}_{i=0}^{K+1}$.

Algorithm 4 Parameterized MLP Forward Pass

Require: Architecture arch $= [d, w, L]$ where d is input/output dimension, w is hidden width, L is number of layers
Require: Input $x \in \mathbb{R}^{n \times d}$, parameter vector $\theta \in \mathbb{R}^p$
Require: Time-varying flag time_varying $\in \{\text{true}, \text{false}\}$

$d_{\text{in}} \leftarrow$ if time_varying $d + 1$ else d ▷ Adjust input dimension
idx $\leftarrow 0$ ▷ Current position in θ
$h \leftarrow x$

// Input Layer
Extract $W_1 \in \mathbb{R}^{w \times d_{\text{in}}}$ from $\theta[\text{idx} : \text{idx} + w \cdot d_{\text{in}}]$
idx $\leftarrow$ idx $+ w \cdot d_{\text{in}}$
Extract $b_1 \in \mathbb{R}^w$ from $\theta[\text{idx} : \text{idx} + w]$
idx $\leftarrow$ idx $+ w$
$h \leftarrow \sigma(W_1 h + b_1)$ ▷ σ is activation function

// Hidden Layers
for $\ell = 2$ **to** $L - 1$ **do**
    Extract $W_\ell \in \mathbb{R}^{w \times w}$ from $\theta[\text{idx} : \text{idx} + w^2]$
    idx $\leftarrow$ idx $+ w^2$
    Extract $b_\ell \in \mathbb{R}^w$ from $\theta[\text{idx} : \text{idx} + w]$
    idx $\leftarrow$ idx $+ w$
    $h \leftarrow \sigma(W_\ell h + b_\ell)$
end for

// Output Layer
Extract $W_L \in \mathbb{R}^{d \times w}$ from $\theta[\text{idx} : \text{idx} + d \cdot w]$
idx $\leftarrow$ idx $+ d \cdot w$
Extract $b_L \in \mathbb{R}^d$ from $\theta[\text{idx} : \text{idx} + d]$
$h \leftarrow W_L h + b_L$ ▷ No activation on output
return h

- **Rule of thumb:** If the potential energy terms are expected to create new modes or dramatically change boundary shapes, increase the hidden dimension.

Neural ODE Integration: Two factors affect forward simulation quality:

- **Solver choice:** We use midpoint integration, as it is standard in flow-based generative models.
- **Integration steps:** 10 steps suffice for most problems. Use at least the number of steps required by your boundary NODEs for accurate sampling from the target distributions.

Action Approximation (Time Steps N): This is an important parameter that controls the temporal discretization accuracy.

Table 2: Action convergence with respect to time discretization steps N.

N	Action	Kinetic Energy	Potential Energy
10	66.06	37.38	28.68
20	42.09	37.77	12.82
30	30.31	29.46	0.788
40	30.20	29.72	0.735
50	30.10	29.37	0.725

Recommendation: Start with N=20 minimum and increase until the action converges (typically N=30-50). The dramatic drop from N=10 to N=20 demonstrates why sufficient discretization is crucial. This parameter is related to the complexity of the problem: longer distances and more complex energy landscapes require finer temporal discretization.

Monte Carlo Samples M: The number of samples M affects the quality of the action estimate. Even for high-dimensional problems (e.g., 50D with M=1000), we maintain solution quality as shown in the Appendix.

Computation of $\log(\rho)$ and $\nabla \log(\rho)$: Following the scaling approach in the CNF literature [4], we use the Hutchinson trace estimator to make the ODE for $\log(\rho)$ computationally tractable. To the best of our knowledge, there are no unbiased estimator techniques for $\nabla \log(\rho)$, and we consider developing such estimators an interesting direction for future work.

F Additional Numerical Results

In this subsection, we report all the experimental details. In Table 4 we report the hyperparameters for the algorithms and the boundary conditions for each problem. The notation [x,y,z] in Table 4 defines the architecture of the networks, x is the input dimension, y is the number of neurons per layer, and z is the number of layers. We assumed the value of the constants $\alpha_0 = \alpha_1$ in Algorithm 2, which we report as α in Table 4.

Here we report that [20] is under CC BY-NC licence, [29] is under CC BY-NC 4.0 License, and [17] has no license.

F.1 Pre-training strategy

F.1.1 Zero initialized boundary parameters

Our framework can use pre-trained parameters θ_0 and θ_1 for the boundary conditions ρ_0 and ρ_1, respectively. To pre-train a parameter, we use Flow Matching (FM) [18] to learn a velocity field to sample from a dataset. The choice of training framework for the boundary parameters motivates to adopt the FM loss function as our dissimilarity metric L. As demonstrated by [6], the FM loss function provides an upper bound on the W_2 distance between the target density and the pushforward density. Therefore, minimizing the FM loss function guarantees the feasibility criteria. The simulation-free training scheme of FM offers a computationally efficient method for pretraining boundary conditions and guaranteeing the feasibility of the boundaries throughout the density path optimization algorithm. In Figure 5a we show the pushforward of the spline obtained from initializing all the control points at $\mathbf{0}$. In Figure 5b we show the resulting optimized path using the PDPO strategy. The running time for this case is 24 m 32s, leading to an action value of 40.31. Since the collocation points are initialized to $\mathbf{0}$, we did not use a geodesic-warmup. Compare this solution with the one reported in Section 4.2.

F.1.2 Reusability of boundary parameters

A crucial feature of PDPO is its boundary parameter reusability: the boundary condition models θ_0 and θ_1 can be trained independently of an action functional's interior dynamics. This independence enables flexible reuse of the boundary parameters.

Specifically, when solving multiple action minimization problems that share boundary constraints, PDPO offers the following flexibility: after training a library of generative models **with shared architecture** $\{\theta_{\rho_1}, \theta_{\rho_2}, \ldots, \theta_{\rho_k}\}$ for distributions $\{\rho_1, \rho_2, \ldots, \rho_k\}$, any action minimization problem

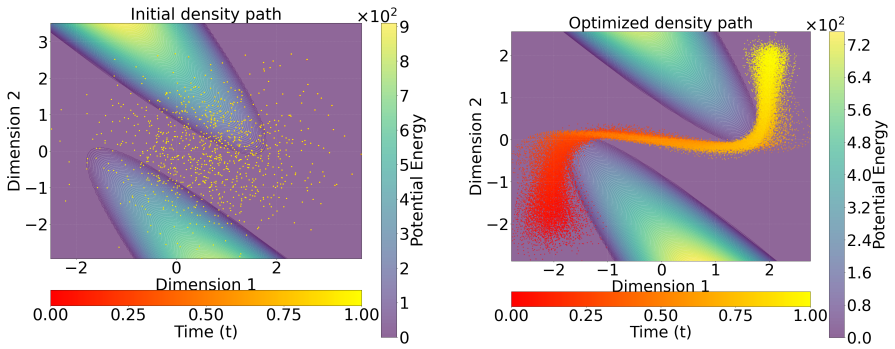

(a) Zero initialized boundaries (b) Optimized path for zero initialized bds

Figure 5: No pertaining for θ_0 and θ_1.

Table 3: Comparison for the SCC problem. The quantities $W_2(\rho_i)$, $i = 0, 1$, denote the empirical Wasserstein-2 distances at times $t = 0$ and $t = 1$, computed using the POT library [12].

Problem (method)	$\mathcal{A}[\rho_t]$	$\int_0^1 \mathbb{E}_{\rho_t}[V(X)]\, dt$	$(W_2(\rho_0),\, W_2(\rho_1))$	Time
SCC (PDPO)	**432.23**	3.42	**(0.12, 0.11)**	**36 m 12 s**
SCC (GSBM)	440.02 ± 0.75	**3.12**	(0.59, 1.76)	53 m 13 s

with boundary conditions in this set can reuse the parameters of the pretrained models, regardless of the direction of transport or the specific action functional. For example, if Problem 1 transports from ρ_i to ρ_j and Problem 2 transports from ρ_j to ρ_i, both problems can use the same pretrained pair $(\theta_{\rho_i}, \theta_{\rho_j})$ by simply swapping their roles as initial and terminal conditions.

This modularity significantly reduces computational cost when solving families of related problems. For instance, in the opinion depolarization example, once θ_0 and θ_1 are trained (29m35s and 31m12s, respectively), they can be reused for alternative action functionals, different polarization dynamics, or even reversed boundary conditions, provided the marginal distributions remain unchanged.

We treat the pretraining phase for the boundary models as a *one-time investment*.

To demonstrate this reusability feature, we reuse the pretrained boundary-condition models from the VNEFI example in a different setting, under a modified action functional and with reversed flow direction. In the VNEFI problem, the boundary conditions are

$$\rho_0 = \mu = \mathcal{N}\left(\begin{bmatrix}-1\\-1\end{bmatrix}, 0.5I\right), \qquad \rho_1 = \nu = \mathcal{N}\left(\begin{bmatrix}1\\1\end{bmatrix}, 0.5I\right).$$

Denote the corresponding pretrained models by θ_μ and θ_ν (training times: 0.38 s and 0.39 s, respectively).

We then apply these same boundary models to solve the **SCC problem** from [20], reversing the flow direction so that $\rho_0 = \nu$ and $\rho_1 = \mu$. Figure 6a shows the pushforward of the control points, Figure 6b the interpolated trajectory, and Figure 6c the corresponding GSBM solution. Quantitative results are provided in Table 3.

As before, PDPO achieves a lower action value and shorter training time than GSBM. It is important to emphasize that the boundary parameters are *reused* from the VNEFI example, so the cost of FM training is *amortized* across problems. Both methods yield similar constraint-violation levels, with GSBM showing a slightly smaller residual.

F.2 Geodesic warmup

In the geodesic warmup, we optimize the linearly initialized control points using Algorithm 1 with $F(\rho) = 0$. This approach effectively reduces the computational cost of our algorithm. As we show in

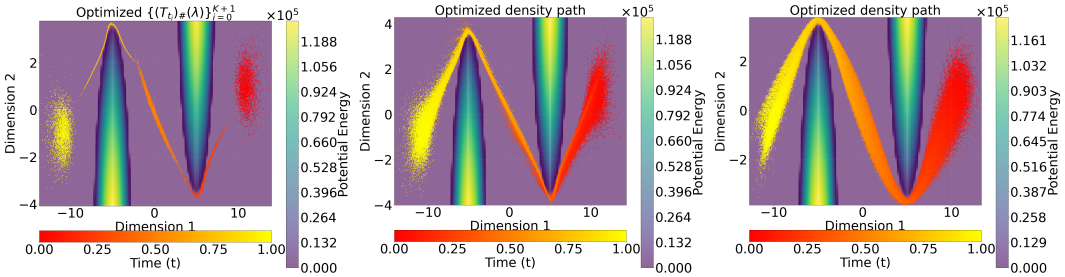

(a) $(T_{\theta_{t_i}})_\#\lambda$ (b) PDPO $(T_{\theta_t})_\#\lambda$ (c) GSBM

Figure 6: Comparison for SCC with new boundary conditions.

Figure 7, using a geodesic warmup drastically improves the speed of convergence and allows PDPO to reach a lower local minimum in the s-curve example.

To reduce the computational cost of the geodesic warmup, we consider at most $N = 15$ points for the trapezoidal rule. The solution computed without geodesic warmup took 5m 32ss, whereas the solution with geodesic warmup took 5m 57s. Thus, the computational overhead of the geodesic warmup is negligible.

In Figure 8, we show a comparison of a solution without geodesic warmup (Figures 8a and 8b) and with geodesic warmup (Figures 8 and 8d).

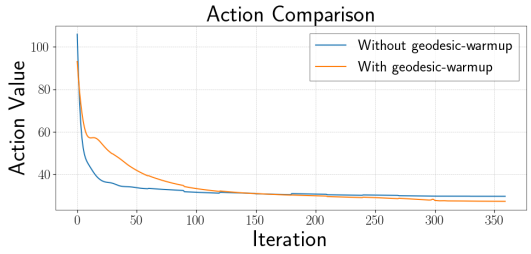

Figure 7: Comparison of action for solutions with and without geodesic warmup.

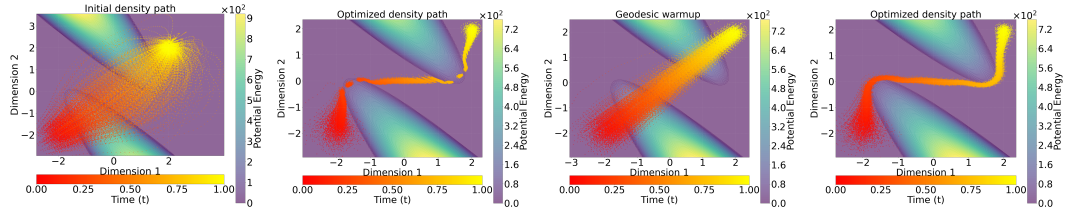

(a) Linear interpolation in parameter space (b) Solution without geodesic warmup (c) Geodesic warmup (d) Solution with geodesic warmup

Figure 8: Comparison of solutions with and without geodesic warmup.

F.3 Ablation Control Points

In Figure 9 we can see the comparison of the difference in the solution obtained by PDPO when varying the number of control points K. As we can see, when the number of control points increases, the quality of the solution also increases. Observe that the transition between the obstacles is smoother as the number of control points increases.

Table 4: Experimental set-up

	GMM	V-neck	S-tunnel	Opinion	
d	2	2	2	2	1000
K	5	3	5	3	3
N	30	60	30	20	20
M	1000	1000	1000	1000	5000
Architecture	[2,256,4]	[2,128,4]	[2,64,4]	[2,128,4]	[1000,128,4]
Epochs	15	15	18	10	10
Coupling opt steps	20	20	20	20	20
Path opt. steps	30	20	30	20	20
Geodesic warmup steps	100	100	100	200	200
α	100000	100000	100000	100000	10000
$(\kappa_0, \kappa_1, \kappa_2)$	(50,0,0)	(3000,50,0)	(100 , 0 ,5)	(0,50,0)	(0,50,0)
Mean ρ_0	$e^{16i\pi}, i = 0, \ldots, 7$	$\begin{bmatrix} -11 \\ -1 \end{bmatrix}$	$\begin{bmatrix} -2 \\ -2 \end{bmatrix}$	$\mathbf{0}$	$\mathbf{0}$
Mean ρ_1	$e^{8i\pi}, i = 0, \ldots, 3$	$\begin{bmatrix} 11 \\ 1 \end{bmatrix}$	$\begin{bmatrix} 2 \\ 2 \end{bmatrix}$	$\mathbf{0}$	$\mathbf{0}$
Covariance of ρ_0	$\mathbf{I}$	$0.5\mathbf{I}$	$0.1\mathbf{I}$	$\mathrm{diag}(\begin{bmatrix} 0.5 \\ 0.25 \end{bmatrix})$	$\mathrm{diag}(\begin{bmatrix} 4 \\ 0.25 \\ \vdots \\ 0.25 \end{bmatrix})$
Covariance of ρ_1	$\mathbf{I}$	$0.5\mathbf{I}$	$0.01\mathbf{I}$	$3\mathbf{I}$	$3\mathbf{I}$

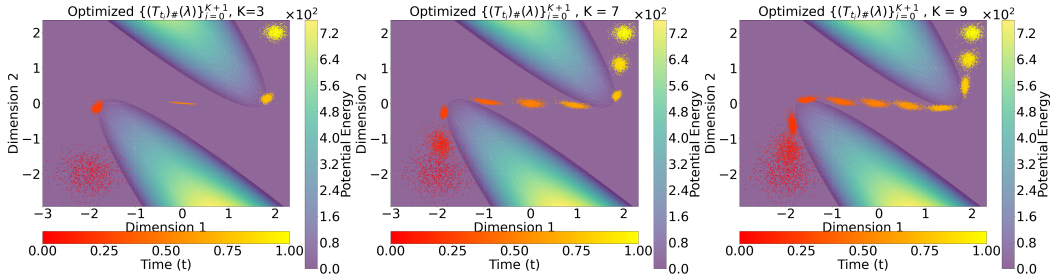

(a) Optimized control points $K = 3$ (b) Optimized control points $K = 7$ (c) Optimized control points $K = 9$

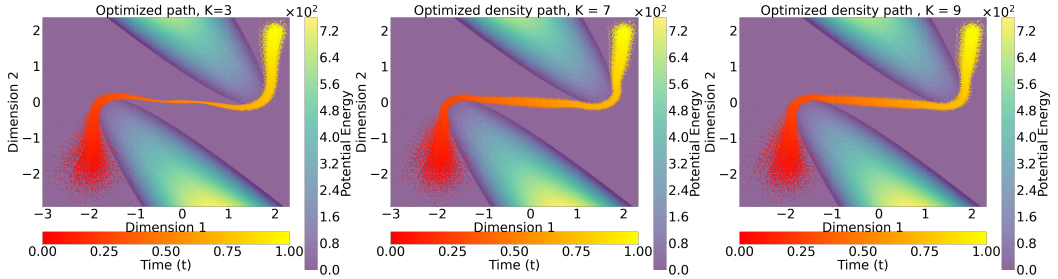

(d) Optimized density path $K = 3$ (e) Optimized density path $K = 7$ (f) Optimized density path $K = 9$

Figure 9: Comparison of solutions with increasing number of control points K.

F.4 Obstacle Avoidance with Mean Field Interactions

Here we provide the definitions for the entropy $\mathcal{E}(\rho)$ and congestion potential $\mathcal{C}(\rho)$,

$$\mathcal{E}(\rho) = \int_{\mathbb{R}^d} \log(\rho)\rho dx \quad \text{and} \quad \mathcal{C}(\rho) = \int_{\mathbb{R}^{d\times d}} \frac{2}{\|x-y\|^2}\rho(x)\rho(y)dxdy.$$

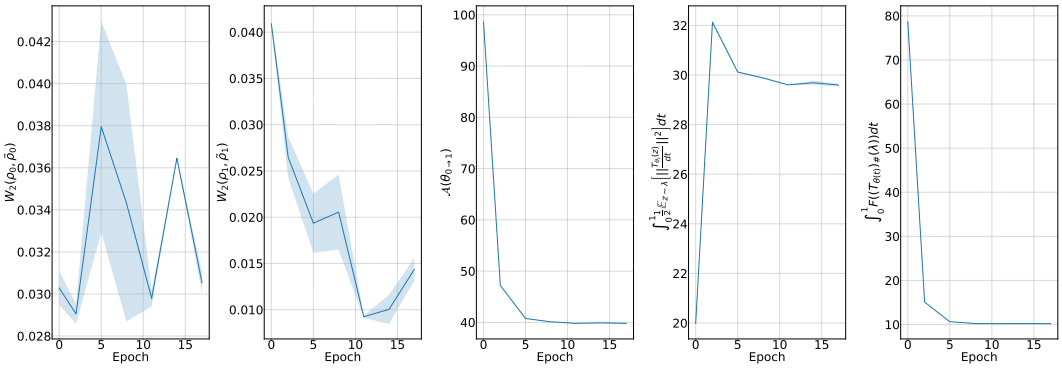

Figure 10: Quantities of interest with uncertainty estimates along the training process, **S-curve**.

Remark: In Table 1 we reported the W_2 distance of the boundaries for GSBM. The samples at the terminal time $t = 1$ are generated by the forward solver, while the samples at the initial time $t = 0$ are produced by the backward solver.

S-curve The definition of the problem and source code were taken from [17]. We refer to it for the definition of the obstacle. APAC-Net was more sensitive to the coefficient κ_0 and κ_2,; there we used $\kappa_0 = 5$ and $\kappa_2 = 1$.. The action reported in Table 1 for APAC-Net was obtained by evaluating its solution using our code with the values of κ_0, κ_2 reported in 4. In Figure 10 we show the W_2 distance with the boundaries, action, kinetic energy, and potential function along the training process. In these plots, an epoch is the completion of coupling + path optimization iterations. In these plots, we can clearly see that the feasibility condition is met from epoch 0 thanks to our pre-training strategy.

Both schedulers in this experiment are StepLR. The learning rate for the coupling optimizer is 10^{-4} with a step size of 10, and $\gamma = 0.9$. The learning rate for the path optimizer is 5×10^{-4}, step size of 10 and $\gamma = 0.1$.

V-Neck The definition and source code were taken from [20]. When GSBM's training time is constrained to match PDPO's training time, its action value is the same as before, but the boundary approximation is noticeably worse, $W_2(\rho_0, \tilde{\rho_0}) = 0.12 \pm 0.002$, $W_2(\rho_1, \tilde{\rho_1}) = 0.107 \pm 0.002$ 1h 15m 24s.

In Figure 12 we report the quantities of interest along the training epochs. See 11 to see the pushforward of the three control points, and the comparison of the PDPO and GSBM solutions.

Both schedulers in this experiment are StepLR. The learning rate for the coupling optimizer is 10^{-4} with a step size of 5, and $\gamma = 0.1$ The learning rate for the path optimizer is 5×10^{-3}, step size of 5 and $\gamma = 0.25$

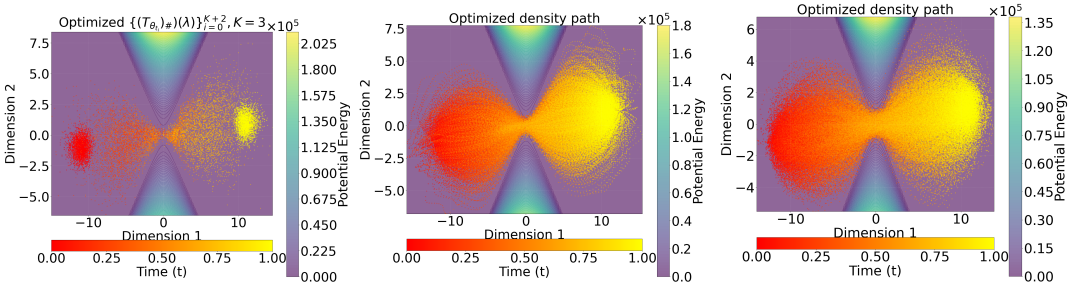

(a) Pushforward with control points (b) PDPO (c) GSBM

Figure 11: V-neck-E-FI a) Pushforward with control points. b) Pushforward with interpolated curve. c) Solution by GSBM.

GMM The definition and source code were taken from [20]. See Figure 13 for the comparison of the solutions. In this example, we use $\lambda = \rho_0$. To guarantee this is satisfied, we define $\theta_0 := \mathbf{0}$, the zero

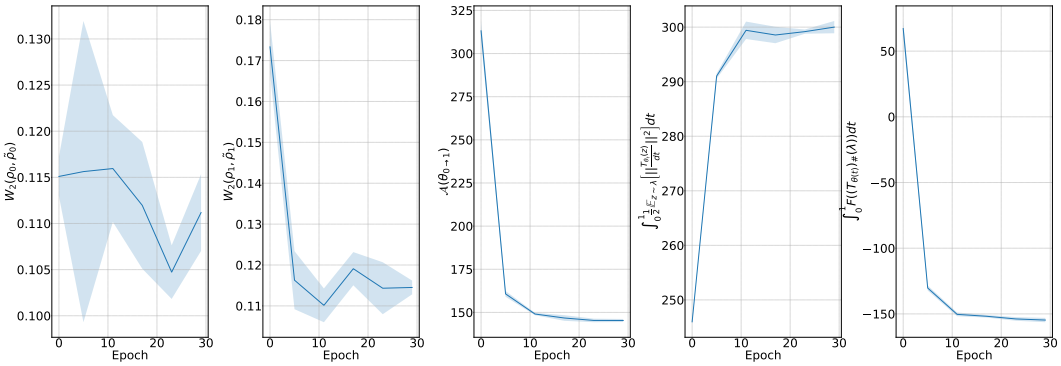

Figure 12: Quantities of interest with uncertainty estimates along the training process, **vneck**

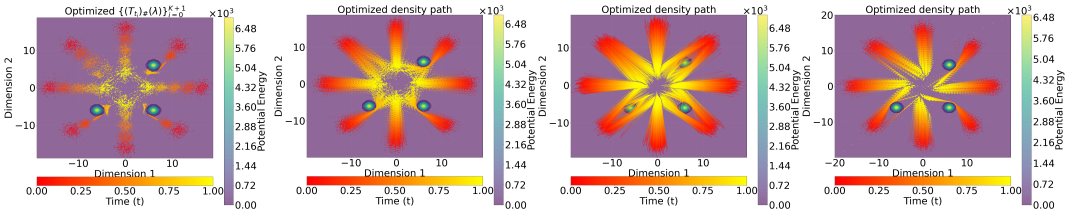

(a) Pushforward with control points (b) PDPO (c) GSBM (d) NLOT

Figure 13: Comparison for GMM example

vector. In Figure 14 we report the quantities of interest along the training epochs. See 13 to see the pushforward of the five control points, and the comparison of the PDPO and GSBM solutions.

The schedulers in this experiment are cosine for the coupling optimization and StepLR for the path optimization. The learning rate for the coupling optimizer is 5×10^{-6}, the setup for the cosine scheduler is $T_0 = 5$, $T_{\text{mult}} = 2$, $\eta_{\min} = 1 \times 10^{-6}$. The learning rate for the path optimization is 0.001, step size of 3, and $\gamma = 0.9$

F.5 Opinion Depolarization

In this problem, opinions $X(t) \in \mathbb{R}^{1000}$ evolve according to a polarizing dynamic:

$$\frac{dx(t)}{dt} = f_{\text{polarize}}(x(t); p_t),$$

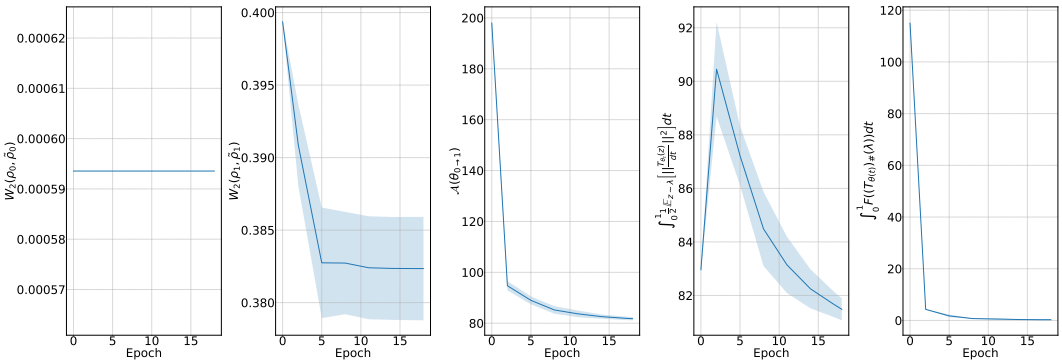

Figure 14: Quantities of interest with uncertainty estimates along the training process, **GMM**

with

$$f_{\text{polarize}}(x; p_t, \xi_t) := \mathbb{E}_{y\sim p_t}[a(x, y, \xi_t)\bar{y}], \quad a(x, y, \xi_t) := \begin{cases} 1 & \text{if sign}(\langle x, \xi_t\rangle) = \text{sign}(\langle y, \xi_t\rangle) \\ -1 & \text{otherwise} \end{cases}.$$

When this dynamic evolves without intervention, opinions naturally segregate into groups with diametrically opposed views. However, the desired outcome is a unimodal distribution.

To solve this problem, we follow [20] and incorporate the polarizing dynamics as a base drift or prior. See [11] for a reference in OT problems with prior velocity fields. Specifically, the action to optimize in the parameter space is defined by

$$\mathcal{A}_{\text{polarize}}(\theta_{0\to 1}) := \mathbb{E}_{z\sim\lambda}\left[\frac{1}{2}\|f_{\text{polarize}}(T_{\theta(t)}(z); (T_{\theta(t)})_{\#}(\lambda)) - \frac{d}{dt}T_{\theta(t)}(z)\|^2\right] + \int_0^1 F((T_{\theta(t)})_{\#}(\lambda))dt.$$

The potential energy term is a congestion cost that encourages particles to maintain a distance from each other. We follow the experimental setup in [20] and [19]. Because of the dimension, we can only simulate deterministic dynamics, as specified in [30]. In Figure 15 we compare the optimized density trajectory and directional similarity histogram. These plots show that both methods obtain a nonpolarized trajectory.

F.6 50D Scrhödinger Bridge

The SB between Gaussians has a closed-form solution [8]. In Table 5, we evaluate PDPO's accuracy by computing two different path discrepancies: $\int_0^1 W_2^2(\rho_{\theta(t)}, \rho(t))dt$ and $\int_0^1 W_2^2(\rho_{\theta(t)}, \tilde{\rho}(t))dt$. Here, $\rho(t)$ represents the theoretical SB solution between the original Gaussian boundaries, $\tilde{\rho}(t)$ is the SB solution between the approximated boundaries $(T_{\theta_0})_{\#}\lambda$ and $(T_{\theta_1})_{\#}\lambda$, and $\rho_{\theta(t)}$ is the density path recovered by PDPO. The first integral measures how closely PDPO approximates the true SB solution, while the second evaluates how well PDPO solves the boundary-approximated problem.

While the tabular results quantify the global accuracy of our method, Figure 16 provides a more intuitive visualization through a 2D projection of sample trajectories. In the figure, blue points represent samples from our PDPO solution $\rho_{\theta(t)}$, green points show the theoretical solution $\rho(t)$, and red points display the boundary-matched solution $\tilde{\rho}(t)$. This visualization demonstrates that PDPO accurately approximates individual particle trajectories throughout the transport process, confirming the effectiveness of our approach even in high-dimensional settings.

Table 5: SB between Gaussians

d	σ	$\int_0^1 W_2^2(\rho_{\theta(t)}, \rho(t))dt$	$\int_0^1 W_2^2(\rho_{\theta(t)}, \tilde{\rho}(t))dt$
50D	1	0.778 ± 0.0018	0.789 ± 0.001

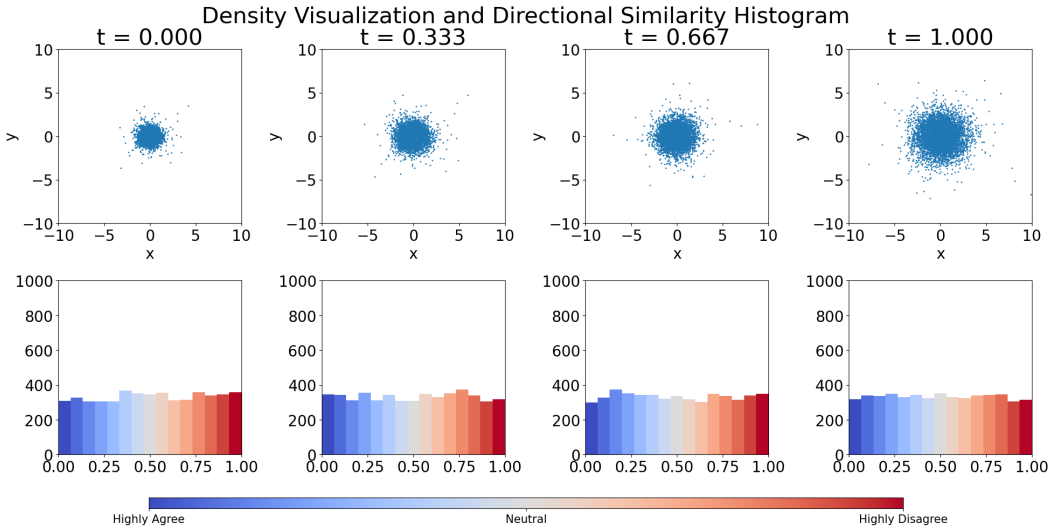

(a) PDPO

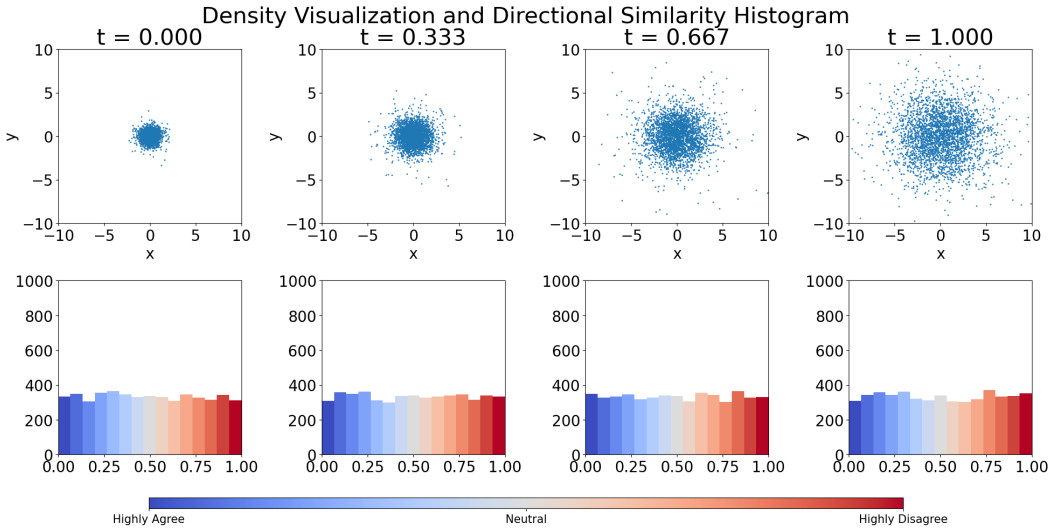

(b) GSBM

Figure 15: Comparison of optimized opinion polarization dynamics.

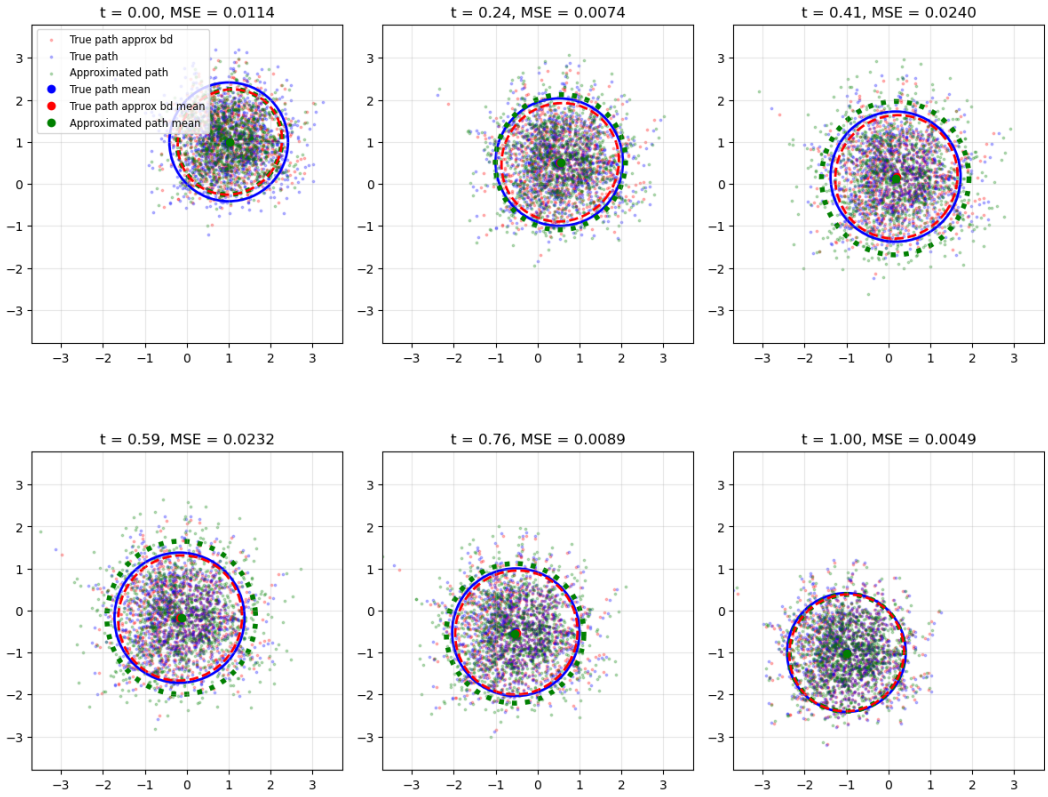

Figure 16: Particle comparison in two random directions.